



NBSIR 84-2912

# The Thermal Response of Aircraft Cabin Ceiling Materials During A Post-Crash, External Fuel-Spill, Fire Scenario

---

Leonard Y. Cooper

U.S. DEPARTMENT OF COMMERCE  
National Bureau of Standards  
National Engineering Laboratory  
Center for Fire Reserch  
Gaithersburg, MD 20899

October 1984

Sponsored by:  
U.S. Department of Transportation  
Federal Aviation Administration  
Technical Center  
Atlantic City Airport, NJ 08405

QC  
100  
.U56  
84-2912  
1984



NBSIR 84-2912

**THE THERMAL RESPONSE OF AIRCRAFT  
CABIN CEILING MATERIALS DURING  
A POST-CRASH, EXTERNAL FUEL-SPILL,  
FIRE SCENARIO**

---

Leonard Y. Cooper

U.S. DEPARTMENT OF COMMERCE  
National Bureau of Standards  
National Engineering Laboratory  
Center for Fire Reserch  
Gaithersburg, MD 20899

October 1984

Sponsored by:  
U.S. Department of Transportation  
Federal Aviation Administration  
Technical Center  
Atlantic City Airport, NJ 08405



---

**U.S. DEPARTMENT OF COMMERCE, Malcolm Baldrige, *Secretary***  
**NATIONAL BUREAU OF STANDARDS, Ernest Ambler, *Director***



## TABLE OF CONTENTS

	<u>Page</u>
List of Figures .....	v
Abstract .....	1
1. INTRODUCTION .....	2
1.1 Purpose of the Investigations .....	2
1.2 Description of the Tests .....	2
2. AN ANALYSIS OF THE THERMAL RESPONSE OF THE CABIN CEILING MATERIAL .....	6
2.1 Components of the Surface Heat Flux .....	6
2.2 Radiation from the Doorway .....	8
2.3 Captured External Fire Product Gases - An Equivalent Buoyant Source .....	9
2.4 Radiation and Convection for the Seating Fire .....	9
2.5 Convective Heat Transfer From a Combined, Equivalent Source of Buoyancy .....	11
2.6 Radiation Between the Lower Ceiling Surface and the Far- Field Cabin Surfaces .....	13
2.7 Heat Transfer from the Upper Ceiling Surface .....	13
2.8 The Boundary Value Problem for the Ceiling, and the Method of Its Solution .....	14
3. CALCULATION OF THE RESPONSE OF THE CEILING IN THE POST-CRASH TEST SIMULATION .....	15
3.1 Calculations for the Test 111 Ceiling Response .....	15
3.2 The Importance of $Q_{equiv}$ .....	16
3.3 Comparisons Between Computed and Measured Temperatures ....	16
4. AN ANALYSIS OF THE THERMAL RESPONSE OF THE NEAR-CEILING THERMOCOUPLES .....	17
4.1 A Model Equation for the Temperature of the Thermocouples .....	17
4.2 Solutions for $T_w$ in the Test 111 Scenario .....	20
4.3 Comparison Between Computed and Measured Temperatures - An Optimum Choice for the Value of $\beta$ .....	20
5. PREDICTING THE POST-CRASH TIME-TO-IGNITION OF CEILING CONSTRUCTIONS IN A FULLY SEATED CABIN .....	21
5.1 Using the Algorithm to Estimate a Measure of Post-Crash Cabin Life Safety .....	21

TABLE OF CONTENTS (continued)

	<u>Page</u>
5.2 Estimates of Post-Crash Fire Growth in Arrays of Cabin Seats .....	22
5.3 Post-Crash Response of a Honeycomb Ceiling Material - Estimates of Time-to-Ignition .....	23
6. SUMMARY AND CONCLUSIONS .....	24
7. ACKNOWLEDGMENTS .....	25
8. REFERENCES .....	26
9. NOMENCLATURE .....	27

LIST OF FIGURES

	<u>Page</u>
Figure 1. A schematic of the test setup .....	29
Figure 2. Measured doorway heat flux vs time (lower fluxmeter ....; upper fluxmeter ____); Test 111 (background) .....	30
Figure 3. Measured doorway heat flux vs time (lower fluxmeter); Tests 104-111 .....	31
Figure 4. Measured temperature vs time at position 1; Tests 104-111 .....	32
Figure 5. Measured temperature vs time at position 2; Tests 104-111 .....	33
Figure 6. Measured temperature vs time at position 3; Tests 104-111 .....	34
Figure 7. Measured temperature vs time at positions 1 (____), 2 (____), and 3 (.....); Test 111 .....	35
Figure 8. A simplified version of the post-crash fire scenario ...	36
Figure 9. The viewfactor between the doorway and a ceiling element .....	37
Figure 10. The idealized post-crash fire scenario .....	38
Figure 11. Computed Test 111 lower ceiling surface temperatures (+: $\beta = 0.$ ; x: $\beta = 3.0 \text{ m}^2$ ) and corresponding, measured near-ceiling temperatures at positions 1, 2, and 3 .....	39
Figure 12. Two extreme configurations for placement of the near-ceiling thermocouples .....	40
Figure 13. Predicted and measured Test 111 thermocouple temperatures ( $\beta = 2.0 \text{ m}^2$ ). <>: predicted $T_w$ , configuration 1 O: predicted $T_w$ , configuration 2 ____, ____ , ____: measured $T_w$ .....	41
Figure 14. Predicted and measured Test 111 thermocouple temperatures ( $\beta = 3.0 \text{ m}^2$ ). <>: predicted $T_w$ , configuration 1 O: predicted $T_w$ , configuration 2 ____, ____ , ____: measured $T_w$ .....	42

LIST OF FIGURES (continued)

	<u>Page</u>
Figure 15. Predicted and measured Test 111 thermocouple temperatures ( $\beta = 4.0 \text{ m}^2$ ). <>: predicted $T_w$ , configuration 1 O: predicted $T_w$ , configuration 2 _____, ---, ____: measured $T_w$ .....	43
Figure 16. Estimate for $\dot{Q}_{\text{seat}}$ for arrays of polyurethane seats with and without blocking layers [13] (--- extrapolated from curves of [13]) .....	44
Figure 17. Predicted lower surface, post-crash, temperature of the honeycomb ceiling material in a cabin outfitted with polyurethane seat cushions; with (____) and without (____) blocking layers .....	45

THE THERMAL RESPONSE OF AIRCRAFT CABIN CEILING MATERIALS DURING  
A POST-CRASH, EXTERNAL FUEL-SPILL, FIRE SCENARIO

Leonard Y. Cooper

Abstract

An algorithm is developed to predict the thermal response of aircraft ceiling materials during a post-crash fire scenario. The scenario involves an aircraft's emergency exit doorway which opens directly onto the flames of an external, fuel-spill fire which engulf a large portion of the fuselage. Data of near-ceiling temperatures acquired during a series of eight, full-scale, wide-body aircraft cabin, post-crash test simulations provide indirect validation of the algorithm. These tests involved cabins outfitted with only single, mockup seats. Two other full-scale cabin tests involving fire spread through twenty-one seat arrays with different types of seat construction provide the input data required to exercise the algorithm in evaluations of fully outfitted cabins.

Relative to the post-crash scenario, a measure of cabin fire safety is proposed, viz., the post-crash time-to-ceiling-ignition. This measure would be used as a surrogate for the post-crash time available for passengers to safely evacuate the cabin. In this sense, the algorithm is exercised in an example evaluation of the fire safety of a candidate honeycomb ceiling material used together in cabin systems involving polyurethane cushion seating, with or without a blocking layer.

## 1. INTRODUCTION

### 1.1 Purpose of the Investigations

The purpose of this investigation is to analyze aircraft cabin ceiling surface temperature data recently acquired during full-scale test simulations of post-crash fires. The analysis is carried out with a view toward the development of a procedure for estimating the temperature histories of overhead aircraft cabin materials subsequent to the ignition of exterior, fuel-spill fires. With such a capability it would be possible to estimate the time for such materials to reach ignition temperatures. This would result in a rational means of ranking the fire safety of candidate overhead aircraft cabin materials.

All tests described here were carried out by staff of the United States (U.S.) Department of Transportation Federal Aviation Administration (FAA) at the National Aviation Facilities Experimental Center, Atlantic City, New Jersey.

### 1.2 Description of the Tests

The experiments involved a wide-body aircraft cabin fire test series similar to those post-crash fire test simulations reported previously in reference [1]\*. The test setup simulated a wide-body aircraft with two open doorways where the fuselage at one of the doorways is engulfed by fire of a

---

\*Numbers in brackets refer to the list of references at the end of this paper.

large, burning, external fuel spill. The fuel-spill fire is simulated by a fire in a 2.44 m x 3.05 m pan of jet fuel (JP-4). The threat to the cabin which would be generated by this external test fire configuration has been shown in [1] to be representative of the threat which would be generated by real, large, external fuel-spill fires. No-wind conditions were simulated during the tests. The actual test article was a surplus U.S. Air Force C133A cargo aircraft with wings and tail surfaces removed.

The ceiling of the test cabin was made up of panels of 0.0127 m thick rigid Kaowool® ceramic fiber board. In the analysis to follow, the thermal properties of this material are assumed to be constant. Consistent with information from the manufacturer, they are taken to be

$$\begin{aligned} \text{thermal conductivity} &= k = 0.045 \text{ W/m}^0\text{K} \\ \text{thermal diffusivity} &= \alpha = 2.67 (10^{-7}) \text{ m}^2/\text{s} \end{aligned} \quad (1)$$

A mockup seat made up of cushions placed on a steel frame was placed in the cabin directly in front of the open doorway which was exposed to the fuel spill fire. The placement was likely to lead to the most rapid ignition of the cushion material. In the present study, data from only eight tests, designated as test numbers 104-111, are considered. The only parameter which was varied from test to test was the seat cushion/fabric construction. One test, test 111, is designated as the background test since it involved the seat frame with no cushioning.

A schematic of the test set up is presented in figure 1.

During the tests the radiant heat flux near the doorway was measured with fluxmeters facing outward toward the pan fire. Measurements were taken at two elevations, 0.30 m and 0.91 m above the floor. At all times during each of the tests the flux measured by the two gages were substantially similar. An example of this can be seen in figure 2 where plots of the two fluxmeter measurements, acquired during the background test, are presented. In the analysis to follow it will be assumed that the radiant flux from the pan fire is uniform and isotropic across the entire doorway. This flux will be taken to be the flux measured by the lower of the two, near-doorway fluxmeters. The measured flux history at this elevation for all eight tests are plotted together in figure 3. This figure provides support for the assumption that the exposure fire was closely reproduced in each of the tests of the series.

This study will consider near-ceiling temperature measurements which were acquired from three thermocouples placed in the line which traverses the width of the cabin and which is directly above the center of the doorway. As noted in figure 1, one of these thermocouples, at designated position 1, was directly above the center of the seat. The other two were 0.91 m (position 2) and 1.83 m (position 3) from the first. The thermocouples were constructed from 24 gage (0.000584 m diameter) chromel/alumel wire. The wire from each of the three thermocouples was supported several centimeters from its bead, and there was an attempt to position the bead close to the ceiling surface with the hope that the bead temperatures would be substantially similar to the respective, nearby, ceiling surface temperatures. Although there was no attempt to measure them, bead-to-ceiling distances were probably of the order of a millimeter. It is noteworthy that the placement of near-ceiling thermocouples in the present test series is different than in previous test series

where thermocouple bead-to-ceiling distances were of the order of a few centimeters.

Except for the background test, data for all tests were available only until 120 s after ignition of the pan fire. The Test 111, background test data were available for 240 s.

Up to 120 s after ignition, the measured temperatures for all eight tests are presented in figures 4-6. Plots of measured temperature vs time at position 1, above the seat, are presented in figure 4. Plots of measured temperature histories at positions 2 and 3 are presented in figures 5 and 6, respectively. As can be seen from these three figures, at each thermocouple location the measured temperature histories are substantially similar for each test. Based on this observation, it is reasonable to assume that, for the threat scenario being simulated and up to the 120 s time mark, fire development in a single, mockup seat would not add significantly to the ceiling surface material fire threat. For this reason, in the analysis of the present test series it is assumed to be adequate to study the thermal response of the ceiling only during the background test. Plots of the temperature histories measured by the three, near-ceiling thermocouples during the background test are presented in figure 7.

## 2. AN ANALYSIS OF THE THERMAL RESPONSE OF THE CABIN CEILING MATERIAL

### 2.1 Components of the Surface Heat Flux

During post-crash fires of the type simulated in the test series there are two major phenomena which can lead to relatively prompt lower surface heating of the cabin ceiling.

The first of these phenomena involves the thick flames and copious products of combustion which engulf the exterior of the fuselage in the vicinity of the threatened, open, cabin doorway. These lead to significant components of both radiant and convective heat flux to the cabin ceiling.

The convective component comes about from the hot, buoyant gases of the fuel spill fire which are captured by the open doorway. Upon entering the cabin, these gases are driven upward toward the ceiling, forming an outward (i.e., away from the doorway and toward the cabin interior) moving ceiling jet. After spreading radially from the doorway, this ceiling jet is redirected away from the general location of the doorway and toward the front and rear of the cabin. Eventually the hot, captured, products of combustion start to fill the cabin. They then participate in venting from the second open doorway and in complicated entrainment processes which develop at the fire-threatened/exposed open doorway itself. (It is noteworthy that a global analysis of the external, fuel spill fire and the captured cabin flow under rather general wind conditions have been presented previously in [2].)

The second phenomenon which leads to heat flux to the lower ceiling surface involves the growing fire which spreads in the cabin seating. As mentioned earlier, the limited, single-seat scenario of the present tests appears to result in only marginally important levels of ceiling heat flux. Yet, as will be discussed later, fire spread in a fully outfitted cabin could indeed lead to a significant additional threat to the cabin ceiling. The seating fire leads to both radiation and convective heating of the ceiling. The radiation would be primarily from the fire's combustion zone, and the convection would result from the fire's plume-driven ceiling jet. This latter ceiling jet would augment the previously mentioned, captured-gas-driven ceiling jet.

Other components of heat flux to/from both the upper and lower ceiling surfaces are radiation from relatively cool, far-field surfaces and reradiation from the ceiling surfaces themselves. Finally, in an analysis of the ceiling heating it is reasonable to account for natural convection cooling of the upper ceiling surface.

For the purpose of analysis the geometry of figure 8, which is somewhat simpler than the actual cabin geometry, will be adopted.

Quantitative estimates for the above components of ceiling heat transfer are developed below. Using these estimates, the boundary value problem for the transient temperature distribution of the ceiling material is then formulated and solved.

## 2.2 Radiation from the Doorway

The entire doorway opening is assumed to be a source of uniform diffuse radiation. The radiant flux emitted from this doorway is assumed to have an amplitude,  $\dot{q}''_{\text{rad-door}}(t)$ , identical to that measured by the lower of the doorway flux calorimeters mentioned earlier.

Any line-of-sight interference by the seats of doorway-to-ceiling radiation will be neglected.

Referring to figure 8, and using a well-known viewfactor result given, e.g., in [3], the viewfactor,  $F_{A-dA}$ , between the area of the doorway opening,  $A$ , and a horizontal element of lower ceiling surface,  $dA$ , lying on a line normal to the plane of the doorway is given by

$$F_{A-dA} = \frac{1}{\pi} \frac{c}{b} (\Gamma_2 \tan^{-1} \Gamma_2 - \Gamma_1 \tan^{-1} \Gamma_1) \quad (2)$$

where

$$\Gamma_1 = b/(a_1^2 + c^2)^{1/2}; \quad \Gamma_2 = b/(a_2^2 + c^2)^{1/2} \quad (3)$$

and where the dimensions  $a_1$ ,  $a_2$ ,  $b$  and  $c$  are defined in figure 9. Thus, the thermal radiant flux from the outside, fuel-spill fire, through the door, and to the ceiling element is taken to be

$$\dot{q}''_{\text{door-ceiling}} = \dot{q}''_{\text{rad-door}} F_{A-dA} \quad (4)$$

### 2.3 Captured External Fire Product Gases - An Equivalent Buoyant Source

The products of combustion of the external, simulated, fuel-spill fire which are captured at the open cabin doorway rise in a plume to the ceiling of the cabin, entraining far-field cabin air during their ascent. In the present analysis the "captured gas" plume will be modeled by a nonradiating, equivalent, point source of buoyancy located at the center of the horizontal surface of the mockup seat, and identified in figure 8. Note that all radiation transfer from the exterior fuel spill fire to the cabin ceiling is assumed to be taken account of in eq. (4). The strength of the equivalent source,  $\dot{Q}_{\text{equiv}}$ , will be assumed to be directly proportional to  $\dot{q}''_{\text{rad-door}}$ . Thus

$$\dot{Q}_{\text{equiv}} = \beta \dot{q}''_{\text{rad-door}} \quad (\beta \text{ in } \text{m}^2) \quad (5)$$

and  $\beta$  is an, as yet undetermined, constant.

As the captured-gas plume impinges on the ceiling near (thermocouple) position 1, it forms an outward moving ceiling jet. As will be described below, estimates of convective heat transfer from this jet to the ceiling surface will make use of the results of [4].

### 2.4 Radiation and Convection for the Seating Fire

During the first 120 s of the post-crash fire, cabin ceiling heat transfer contributions from the burning single mockup cabin seat did not appear to be significant. However, in fully outfitted cabins, it is anticipated that this situation would be changed especially after the first minute

or two subsequent to ignition. This is the case since, by these times, fires in FAA, multiple-seat, cabin test configurations have been observed to grow and spread beyond single seat involvement. Since the present analysis will be extended to fully outfitted cabin scenarios, ceiling heat transfer with an important contribution from the seating fire will be included here at the outset.

The seating fire is simulated by a time-dependent point source of energy release rate,  $\dot{Q}_{\text{seat}}$ , which is assumed to be located, together with the non-radiating source,  $\dot{Q}_{\text{equiv}}$ , at the center of the horizontal surface of the outer, external-fire-exposed, doorway seat. In contrast to  $\dot{Q}_{\text{equiv}}$ , a nonzero fraction,  $\lambda_{r,\text{seat}}$ , of  $\dot{Q}_{\text{seat}}$  is assumed to be radiated uniformly over a sphere surrounding the combustion zone, and to the far field. The remaining rate-of-energy release,  $(1 - \lambda_{r,\text{seat}}) \dot{Q}_{\text{seat}}$ , drives the buoyant fire plume upward. Thus, the radiation from the seating fire which is incident on the ceiling is assumed to be

$$\dot{q}_{\text{rad-seat}}'' = \lambda_{r,\text{seat}} \dot{Q}_{\text{seat}} / [4\pi H^2 (1 + r^2/H^2)^{3/2}] \quad (6)$$

where, as defined in figure 8, H is the source-to-ceiling distance and r is the radial distance from the source as measured along the ceiling.

$\dot{Q}_{\text{seat}}$  would vary from one seat cushion construction to another.  $\dot{Q}_{\text{seat}}$  would typically have to be estimated from test data, and then specified in the present analysis.  $\lambda_{r,\text{seat}}$  would also vary somewhat from one construction to another, although it is reasonable to choose the value  $\lambda_{r,\text{seat}} = 0.35$ , a value which characterizes the radiation from flaming combustion zones of many

practical fuel assemblies [5]. In all calculations to be presented here, the 0.35 value will be adopted.

## 2.5 Convective Heat Transfer From a Combined, Equivalent Source of Buoyancy

A single point source of buoyancy,  $\dot{Q}$ , is used to describe the total generation of upward moving combustion gases which are driven by a combination of the equivalent, captured-gas-buoyancy source,  $\dot{Q}_{\text{equiv}}$ , and the seating-fire-buoyancy source,  $(1 - \lambda_{r,\text{seat}}) \dot{Q}_{\text{seat}}$ . Thus

$$\dot{Q} = \dot{Q}_{\text{equiv}} + (1 - \lambda_{r,\text{seat}}) \dot{Q}_{\text{seat}} \quad (7)$$

All convective heat transfer to the cabin ceiling will be modeled by a  $\dot{Q}$ -generated, plume-driven, ceiling jet. This heat transfer will be estimated with the use of the algorithm, reproduced below, which was developed in [4], and used in [6]. Thus, the convective rate of heat transfer to the ceiling surface will be estimated from

$$\dot{q}''_{\text{conv,L}} = h_L (T_{\text{ad}} - T_{s,L}) \quad (8)$$

In the above,  $T_{s,L}$  is the instantaneous, absolute temperature of the lower ceiling surface,  $T_{\text{ad}}$  is the absolute temperature that would be attained by the lower surface of an adiabatic ceiling,

$$\frac{(T_{\text{ad}} - T_{\text{amb}})}{T_{\text{amb}} \dot{Q}^{*2/3}} = \begin{cases} 10.22 \exp(-1.77 r/H), & 0 \leq r/H \leq 0.75 \\ 2.10 (r/H)^{-0.88}, & 0.75 \leq r/H \end{cases} \quad (9)$$

$\dot{Q}^*$  is a dimensionless buoyant source strength,

$$\dot{Q}^* = \dot{Q} / (\rho_{\text{amb}} C_p T_{\text{amb}} g^{1/2} H^{3/2}) \quad (10)$$

$g$  is the acceleration of gravity, and  $\rho_{\text{amb}}$ ,  $T_{\text{amb}}$  and  $C_p$  are the density, absolute temperature and specific heat, respectively, of the ambient air.

Also,  $h$  is the heat transfer coefficient

$$h_L / \tilde{h} = \begin{cases} 7.75 \text{ Re}^{-0.5} [1 - (5.0 - 0.390 \text{ Re}^{0.2})(r/H)], & 0 \leq r/H \leq 0.2 \\ 0.213 \text{ Re}^{-0.3} (r/H)^{-0.65}, & 0.2 \leq r/H \leq 1.03 \\ 0.217 \text{ Re}^{-0.3} (r/H)^{-1.2}, & 1.03 \leq r/H \end{cases} \quad (11)$$

where

$$\begin{aligned} \tilde{h} &= \rho_{\text{amb}} C_p g^{1/2} H^{1/2} \dot{Q}^{*1/3} \\ \text{Re} &= g^{1/2} H^{3/2} \dot{Q}^{*1/3} / \nu \end{aligned} \quad (12)$$

and  $\nu$  is the kinematic viscosity of the ambient air.

The above algorithm will be used in the present calculations. In doing so, two major assumptions are made; namely 1) effects of the inevitable, growing, upper-cabin smoke layer are relatively weak during the early times of interest, and 2) the interactions of the ceiling jet and lateral cabin wall surfaces, especially surfaces immediately to the doorway side of the plume-ceiling impingement point will not lead to total, instantaneous, heat transfer flux amplitudes which are significantly larger than peak, instantaneous values that will be estimated with their neglect.

## 2.6 Radiation Between the Lower Ceiling Surface and the Far-Field Cabin Surfaces

At all times subsequent to ignition, the lower ceiling surface at temperature  $T_{s,L}$  is assumed to diffusely radiate to the initially ambient temperature, illuminated surfaces of the cabin and its furnishings. In response to this radiation, the temperatures of those lower surfaces outside of the seating combustion zone also increase with time. However, for times of interest here, it is assumed that these latter temperature increases above  $T_{amb}$  are always relatively small compared to the characteristic increases of  $T_{s,L}$ . Accordingly, at a given radial position of the lower ceiling surface, the net radiation exchange between the ceiling and the nonburning surfaces below can be approximated by a net reradiation flux

$$\dot{q}''_{rerad,L} = \epsilon_L \sigma (T_{s,L}^4 - T_{amb}^4) \quad (13)$$

where  $\sigma$  is the Stephan-Boltzmann constant, and  $\epsilon_L$  is the emittance/absorptance of the assumed grey, lower ceiling surface.

## 2.7 Heat Transfer from the Upper Ceiling Surface

Heat is transferred through the ceiling, and eventually the temperature of its upper surface, which is also assumed to be exposed to a constant  $T_{amb}$  environment, begins to rise.

The rate of heat transfer from the upper ceiling surface has convective and radiative components,  $\dot{q}''_{conv,U}$  and  $\dot{q}''_{rerad,U}$ , respectively. These can be estimated from

$$\begin{aligned} \dot{q}''_{\text{conv},U} &= h_U (T_{s,U} - T_{\text{amb}}) \\ \dot{q}''_{\text{rerad},U} &= \epsilon_U \sigma (T_{s,U}^4 - T_{\text{amb}}^4) \end{aligned} \quad (14)$$

where  $T_{s,U}$  is the instantaneous upper surface temperature,  $h_U$  is an effective heat transfer coefficient, and  $\epsilon_U$  is the emittance/absorptance of the assumed grey, upper ceiling surface. The value for  $h_U$  to be used in the present calculations will be [7]

$$h_U = 1.675 |T_{s,U} - T_{\text{amb}}|^{1/3} \text{ W/m}^2 \text{ (T in } ^\circ\text{K)} \quad (15)$$

## 2.8 The Boundary Value Problem for the Ceiling, and the Method of Its Solution

The absolute temperature field of the ceiling material is assumed to be governed by the Fourier heat conduction equation. Initially, the ceiling is taken to be of uniform temperature,  $T_{\text{amb}}$ . The net rates of heat transfer to the lower and upper surfaces,  $\dot{q}''_L$  and  $\dot{q}''_U$ , respectively, are given by

$$\begin{aligned} \dot{q}''_L &= \dot{q}''_{\text{door-ceiling}} + \dot{q}''_{\text{rad-seat}} + \dot{q}''_{\text{conv},L} - \dot{q}''_{\text{rerad},L} \\ \dot{q}''_U &= -\dot{q}''_{\text{conv},U} - \dot{q}''_{\text{rerad},U} \end{aligned} \quad (16)$$

For times of interest here, radial gradients of variables of the problem are assumed to be small enough so that conduction in the ceiling is quasi-one dimensional in space, i.e.,  $T = T(Z, t; r)$ , where  $Z$  is the indepth ceiling coordinate.

An illustration of the final, idealized, post-crash fire scenario to be analyzed here is presented in figure 10.

A computer program for solving the above problem was developed. The solution to the heat conduction equation for the ceiling at every radial position of interest is by finite differences. The algorithm for this was taken from [8] and [9]. For a given calculation,  $N \leq 20$  equally spaced points are positioned at the surfaces and through the thickness of the ceiling. The spacing of these,  $\delta Z$ , is selected to be large enough (based on a maximum time step) to insure stability of the calculation. Throughout a calculation, the change in time for all time steps is made small enough so that, at a given lower surface node, the temperature increase from time step to time step never exceeds one percent of the current value of T at that node.

### 3. CALCULATION OF THE RESPONSE OF THE CEILING IN THE POST-CRASH TEST SIMULATION

#### 3.1 Calculations for the Test 111 Ceiling Response

The algorithm described in the last section was used to predict the ceiling response during the first 240 s of the Test 111, post-crash simulation.

Eq. (1) values of  $k$  and  $\alpha$  were used for the 0.0127 m thick Kaowool® ceiling. The ceiling surfaces were assumed to absorb and radiate as black bodies ( $\epsilon_U = \epsilon_L = 1$ ). Consistent with previous discussion, for this test  $\dot{Q}_{\text{seat}}$  of eq. (6) was taken to be identically zero, and  $\dot{q}''_{\text{rad-door}}(t)$  of eq. (5) was taken to be identical to the Test 111, underseat fluxmeter measurements. Ceiling temperatures at positions 1, 2 and 3 were computed for different  $\beta$ 's in the range  $0 \leq \beta \leq 6.0 \text{ m}^2$ . (This range of  $\beta$  leads to the approximate  $\dot{Q}_{\text{equiv}}$  range  $0 \leq \dot{Q}_{\text{equiv}} \leq 300 \text{ kW}$ .)

The computed lower ceiling histories for  $\beta = 0.$  and  $3.0 \text{ m}^2$  are plotted in figure 11 together with the corresponding, measured, near-ceiling temperatures of figure 7.

### 3.2 The Importance of $\dot{Q}_{\text{equiv}}$

If convective ceiling heating from doorway-captured products of combustion is equivalent to a near-seat buoyancy source of the order of a few hundred kW, then the calculated results plotted in figure 11 indicate that such heating is not significant compared to doorway radiation. (Note that  $\beta = 0.$  and  $3.0 \text{ m}^2$  of figure 11 leads to a  $\dot{Q}_{\text{equiv}}$  of zero and approximately 150 kW, respectively. Also, except for the very earliest few seconds subsequent to ignition, convection from the relatively weak source associated with  $\beta = 3.0 \text{ m}^2$  is seen to lead to net cooling of the strongly irradiated ceiling surface.) This result is consistent with earlier observations where variations in single seat cushion construction (peak energy release rates likely never exceeding the few hundred kW level) did not lead to significant differences in near-ceiling temperature measurements (see figures 4-6).

### 3.3 Comparisons Between Computed and Measured Temperatures

As can be seen in figure 11 the peak computed values of ceiling temperature compare favorably with the corresponding peak temperatures measured by the near-ceiling thermocouples. However, the basic qualitative characteristics of the computed and measured transient thermal responses are significantly different. In particular, the measured temperatures of the thermocouples do not have the same type of rapid response which the numerical solution

properly predicts for the lower ceiling surface temperatures. Also, the close tracking of the position 2 and 3 thermocouples at early times does not compare favorably with a like tracking of the computed, lower ceiling temperatures at these two positions.

Two conclusions result from these observations; namely, the thermocouples are not measuring the temperature of the near-by ceiling surface, and, therefore, data to support the validity of the analysis are not evident. As a result of these conclusions an analysis of the response of the thermocouples was carried out. This analysis, to be reported in the next section, had a two-fold purpose; first, to explain the measured thermocouple responses, and second, to bring a measure of experimental validation, albeit indirect, for the predicted ceiling response.

#### 4. AN ANALYSIS OF THE THERMAL RESPONSE OF THE NEAR-CEILING THERMOCOUPLES

##### 4.1 A Model Equation for the Temperature of the Thermocouples

The objective of the present analysis is to predict the thermal response of the thermocouples when appropriately placed within the figure 10 scenario, near, but not touching the ceiling. The procedure for positioning these devices prior to testing was such that the thermocouple wires were essentially parallel to the lower ceiling surface and at a distance,  $d$ , of the order of 0.001 m. The actual orientation of the 24 gage (diameter = 0.000584 m) wire relative to the doorway plane is unknown. As depicted in figure 12, the analysis will consider two extreme configurations for the wire, viz., normal and parallel to the doorway.

The characteristic time for<sup>1</sup> conductive heat transfer through the wire thickness is relatively small, of the order of tenths of a second. The analysis will therefore assume that throughout the experiment the wire is spatially uniform in temperature.

The density and specific heat of the chromel/alumel wire (a 95 percent Nickel alloy) will be taken to be identical to that of Nickel, viz.,

$$\text{density} = \rho = 8800 \text{ kg/m}^3$$

$$\text{specific heat} = C_p = 460 \text{ Ws/(kg}^0\text{K)}$$

From references [4] and [10] or from reference [11] it is possible to conclude that the thickness of the ceiling jet within which the thermocouples are submerged are of the order of several centimeters. With a characteristic thermocouple-to-ceiling separation distance,  $d$ , of the order of 0.001 m, it is therefore reasonable to assume that gas velocities local to the thermocouple wire are so small that forced convection heating compared to radiative heating of the wire is negligible. On account of the fineness of the wire, the characteristic Grashoff numbers would be relatively small, and it is also reasonable to neglect natural convection heating of the thermocouples.

The thermal analysis which emerges from the above discussion leads to the following equation for the temperature,  $T_w$ , of the thermocouple wire

$$\frac{\pi}{4} \rho C_p D \frac{dT_w}{dt} = \dot{Q}'_{\text{door-wire}} + \dot{Q}'_{\text{ceiling-wire}} + \dot{Q}'_{\text{amb-wire}} - \dot{Q}'_{\text{wire}} \quad (17)$$

where

$$\begin{aligned}\dot{Q}'_{\text{wire}} &= \text{reradiation from the wire, per unit length of wire} & (18) \\ &= \pi D \sigma T_w^4\end{aligned}$$

$$\begin{aligned}\dot{Q}'_{\text{amb-wire}} &= \text{radiation from lower ambient temperature surfaces to} & (19) \\ &\text{the wire, per unit length of wire} \\ &= \frac{\pi D}{2} \sigma T_{\text{amb}}^4\end{aligned}$$

$$\begin{aligned}\dot{Q}'_{\text{ceiling-wire}} &= \text{radiation from the ceiling to the wire,} & (20) \\ &\text{per unit length of wire} \\ &= \frac{\pi D}{2} \sigma T_{s,L}^4\end{aligned}$$

$$\begin{aligned}\dot{Q}'_{\text{door-wire}} &= \text{radiation from the doorway to the wire,} & (21) \\ &\text{per unit length of wire} \\ &= \alpha D \dot{q}''_{\text{door-ceiling}}\end{aligned}$$

In eq. (21),  $\dot{q}''_{\text{door-ceiling}}$  is given in eq. (4), and, depending on the wire configuration,

$$\begin{aligned}\alpha &= 1 \text{ for wire normal to the door plane, i.e., configuration 2} \\ &\text{of figure 12.} & (22)\end{aligned}$$

$$\begin{aligned}\alpha &\approx 1/\sin\theta \text{ (see figure 9 for definition of } \theta) \text{ for wire parallel} \\ &\text{to the door plane, i.e., configuration 1 of figure 12.}\end{aligned}$$

In the above, all surfaces are assumed to radiate and absorb as black surfaces.

To obtain a solution for the  $T_w$  of a thermocouple at a given position along the cabin ceiling one would specify  $\alpha$  and  $T_{s,L}(t)$  at that position, use the measured values of  $\dot{q}''_{\text{rad-door}}$  to obtain  $\dot{q}''_{\text{door-ceiling}}$ , and solve eq. (17) subject to the initial condition  $T_w(t = 0) = T_{\text{amb}}$ .

## 4.2 Solutions for $T_w$ in the Test 111 Scenario

The above procedure for predicting  $T_w(t)$  was applied to the Test 111 scenario. The analysis was carried out numerically for a thermocouple in position 1, 2 or 3 and in configuration 1 or 2. In each case, the history for  $T_{s,L}(t)$ , which was required in the analysis, was taken from the ceiling temperature calculations described earlier.

The results of the  $T_w$  calculations are presented in figures 13, 14, and 15 for  $\beta$  values of 2.0 m<sup>2</sup>, 3.0 m<sup>2</sup>, and 4.0 m<sup>2</sup>, respectively. Also included in these figures are plots of the measured  $T_w$  values previously presented in figures 7 and 8.

## 4.3 Comparison Between Computed and Measured Temperatures - An Optimum Choice for the Value of $\beta$

As can be seen in figures 13-15, the computed and measured thermocouple temperatures compare as favorably as one could reasonably hope for in an analysis of the kind of experimental fire scenario under investigation.

Perhaps of greatest significance is the early-time thermocouple temperature predictions, which were of particular concern in the previous ceiling temperature - thermocouple temperature comparisons of figure 11. Here, the simulations of the early, near-linear responses of the thermocouples are noteworthy.

Of further significance is the fact that the results of the calculations reveal a possible explanation for the previously noted, close tracking of the

response of the thermocouples at positions 2 and 3. As can be observed in each of the three figures, the present analysis predicts such behavior if the thermocouple wire at position 2 was normal to the door plane (configuration 2), and the thermocouple wire at position 3 was parallel to the door plane (configuration 1).

Figures 13-15 provide a basis for selecting the "best" value for  $\beta$  with which to carry out the ceiling temperature calculation in the context of the post-crash cabin fire scenario under investigation. In this regard, the  $\beta$  predicting a ceiling response which, in turn, yields the most favorable comparisons between calculated and measured values of  $T_w$  would be the obvious choice. As is evident from the figures, the  $T_w$  predictions are not very sensitive to  $\beta$  variations in the appropriate range 2.0-4.0  $m^2$ . Furthermore, of the values  $\beta = 2.0 m^2$ ,  $3.0 m^2$ , and  $4.0 m^2$ , all yield reasonable  $T_w$  predictions, and no one of these values clearly yields more favorable  $T_w$  predictions than the others.  $\beta = 3.0 m^2$  will be chosen as the "best" value.

## 5. PREDICTING THE POST-CRASH TIME-TO-IGNITION OF CEILING CONSTRUCTIONS IN A FULLY SEATED CABIN

### 5.1 Using the Algorithm to Estimate a Measure of Post-Crash Cabin Life Safety

The results of the previous section provide some confidence in the post-crash ceiling thermal response algorithm. To use the algorithm in a manner that would simulate the post-crash fire exposure of a fully seated cabin, it is necessary to include the effects of fire spread in an array of seating adjacent to the exposed, open doorway. As was discussed earlier, this would be done by inputting appropriate, nonzero,  $\lambda_{r,seat}$  and  $\dot{Q}_{seat}$  terms in eqns. (6)

and (7). Then, using the  $k$  and  $\alpha$  of a candidate ceiling material, the algorithm would calculate the ceiling's time-dependent, post-crash, thermal response.

In the most likely case of a combustibile ceiling material, one could, for example, predict the time for the lower surface to reach a characteristic ignition temperature. Since cabin flashover would not likely occur prior to ceiling ignition, such a time-to-ignition would provide a reasonable measure of post-crash cabin fire safety, viz., the minimum time available for passengers to evacuate the cabin or the Available Safe Egress Time (ASET) [12]. Hopefully, evaluations of practical cabin ceiling material candidates would lead to associated ignition times, or minimum ASET's, which exceed the time required for cabin evacuation. In any event, the greater the time-to-ignition of a material the better.

In the case of a noncombustible ceiling, time-to-ignition in the above discussion would be replaced by time to reach some agreed upon ceiling temperature (e.g., 600°C), which would typically be associated with cabin flashover.

## 5.2 Estimates of Post-Crash Fire Growth in Arrays of Cabin Seats

The objective of reference [13] was to obtain estimates of the energy release rate of post-crash fires growing through arrays of cabin seats. Based on FAA, full-scale, 21 seat tests which were similar to Tests 104-111, estimates of fire growth in two types of seat construction were obtained. The first type of seats, designated as "regular" seats were made of fire retarded polyurethane foam covered with wool-nylon fabric. The second seat construc-

tion was similar to the first, except that it included a blocking layer constructed of a 0.0048 m thick sheet of neoprene with a polyester scrim.

The estimates of  $\dot{Q}_{\text{seat}}(t)$  for the two types of seats are plotted in figure 16. The plots terminate at times 140 s and 185 s, at which times video-tape recordings of the tests indicated the initiation of either flash-over (the 140 s time) or of rapid development of total obscuration (the 185 s time).

The  $\dot{Q}_{\text{seat}}$  estimates of figure 16 will be used below to evaluate the post-crash response of a specific, honeycomb ceiling material.

### 5.3 Post-Crash Response of a Honeycomb Ceiling Material - Estimates of Time-to-Ignition

The algorithm developed here was used to estimate the post-crash thermal response of a 0.0254 m thick, honeycomb composite, aircraft lining material with an epoxy fiberite covering. The effective thermal properties of the composite were measured, and found to be [14]

$$\begin{aligned}
 k &= 5.9 (10^{-5}) \text{ kW}/(\text{m}^0\text{K}) \\
 \alpha &= 4.8 (10^{-7}) \text{ m}^2/\text{s} \\
 \rho &= 110. \text{ kg}/\text{m}^3 \\
 C_p &= 1.11 \text{ kJ}/(\text{kg}^0\text{K})
 \end{aligned}
 \tag{23}$$

$\lambda_{r,\text{seat}}$  of eq. (7) was taken to be 0.35 and  $\dot{Q}_{\text{seat}}$  was simulated by the plots of figure 16. The computer program written to exercise the algorithm was actually designed to accept pairs of  $[t, \dot{Q}_{\text{seat}}(t)]$  data points as input,

and then to linearly interpolate between these to obtain  $\dot{Q}_{\text{seat}}$  at any arbitrary time during the calculation.  $\beta$  of eq. (5) was taken to be  $3.0 \text{ m}^2$ .  $\epsilon_L$  and  $\epsilon_U$  were taken to be 1.

The predicted history of the lower surface of the honeycomb ceiling directly above the doorway seat is plotted in figure 17 for both "regular" seating and "blocked" seating.

The ignition temperature,  $T_{\text{ign}}$ , of the honeycomb material had been measured previously, and was found to be [15]

$$T_{\text{ign}} = 536^{\circ}\text{C} \quad (24)$$

As can be seen in figure 17 the calculation predicts onset of ceiling ignition at 148 and 204 s for "regular" and "blocked" seating, respectively. For cabins outfitted with ceilings of the honeycomb material, the use of the blocked rather than the unblocked seating construction would lead to a 56 s advantage in time available for post-crash cabin evacuation.

## 6. SUMMARY AND CONCLUSIONS

An algorithm was developed to predict the thermal response of aircraft ceiling materials during a specific, post-crash, external fuel-spill, fire scenario. Experimental measurements of near-ceiling temperatures in a series of eight, full-scale, post-crash, single seat, test simulations provided indirect validation of the algorithm. Two other full-scale tests, each of which involved fire spread through arrays of seating with different types of

seat construction (fire retarded polyurethane foam covered with a wool-nylon fabric, with and without a neoprene sheet-polyester scrim blocking layer) provided the input data required to exercise the algorithm.

The post-crash, time-to-ignition of a ceiling construction, which can be associated with the time available for passengers to safely evacuate an aircraft, was recommended as one possible measure of the fire safety of the cabin ceiling-seat construction system (i.e., changing either the ceiling or the seat-construction has an impact on cabin fire safety).

Relative to the post-crash fire scenario considered here, the algorithm was used to predict the response of a candidate honeycomb ceiling material when used in a wide-body aircraft, with and without seat blocking. Times-to-ceiling ignition were estimated to be 148 and 204 s with and without seat blocking, respectively.

In a similar way, the algorithm developed here could be used to estimate the time-to-ignition of any other candidate ceiling material which would be used in cabins having either blocked or unblocked seating. Required inputs are the thickness and the effective thermal conductivity and diffusivity of the material.

## 7. ACKNOWLEDGMENTS

This work was supported by the Federal Aviation Administration of the U.S. Department of Transportation.

## 8. REFERENCES

- [1] Hill, R.G., Johnson, G.R. and Sarkos, C.P., Postcrash Fuel Fire Hazard Measurements in a Wide-Body Aircraft Cabin, FAA-NA-79-42, Federal Aviation Admin., NAFEC, Atlantic City, NJ, 1979.
- [2] Emmons, H.W., The Ingestion of Flames and Fire Gases Into a Hole in an Aircraft Cabin for Arbitrary Tilt Angles and Wind Speed, Home Fire Proj. Rpt. 52, Harvard Univ. Div. Appl. Sciences, Cambridge, MA, 1982.
- [3] Eckert, E.R.G. and Drake, R.M., Heat and Mass Transfer, McGraw-Hill, 2nd Ed., 1959.
- [4] Cooper, L.Y., Heat Transfer from a Buoyant Plume to an Unconfined Ceiling, J. Heat Transfer, 104, p. 446, 1982.
- [5] Cooper, L.Y., A Mathematical Model for Estimating Available Safe Egress Time in Fires, Fire and Materials, 6, p. 135, 1982.
- [6] Cooper, L.Y., Thermal Response of Unconfined Ceilings Above Growing Fires and the Importance of Convective Heat Transfer, 22nd National Heat Transfer Conf., ASME Paper 84-HT-105, 1984 and NBSIR 84-2856, National Bureau of Standards, Washington, DC, 1984.
- [7] Yousef, W.W., Tarasuk, J.D. and McKeen, W.J., Free Convection Heat Transfer from Upward-Facing, Isothermal, Horizontal Surfaces, J. Heat Transfer, 104, p. 493, 1982.
- [8] Emmons, H.W., The Prediction of Fires in Buildings, 17th Symp. (Inter.) on Combustion, p. 1101, 1979.
- [9] Mitler, H.E. and Emmons, H.W., Documentation for the Fifth Harvard Computer Fire Code, Home Fire Project Tech. Rpt. 45, Harvard Univ., Cambridge, MA, 1981.
- [10] Poreh, M., Tsuei, Y.G. and Cermak, J.E., Investigation of a Turbulent Radial Wall Jet, ASME Journal of Applied Mechanics, p. 457, 1967.
- [11] Alpert, R.L., Turbulent Ceiling-Jet Induced by Large-Scale Fires, Combustion Science and Technology, Vol. 11, p. 197, 1975.
- [12] Cooper, L.Y., A Concept of Estimating Safe Available Egress Time, Fire Safety Journal, Vol. 5, p. 135, 1983.
- [13] Steckler, K., National Bureau of Standards, Chapter 1 of the Role of Aircraft Panel Materials in Cabin Fires and Their Properties, Quintiere et al, to appear as NBSIR, National Bureau of Standards, Washington, DC.
- [14] Parker, W., National Bureau of Standards, private communication.
- [15] Harkleroad, M., Quintiere, J. and Walton, W., Radiative Ignition and Opposed Flame Spread Measurements on Materials, DOT/FAA/CT-83/28 (National Bureau of Standards Rpt. to) Federal Aviation Admin., Atlantic City, NJ, 1983.

## 9. NOMENCLATURE

$a_1, a_2, b, c$	dimensions, Fig. 9
$C_p$	specific heat
$D$	wire diameter
$F_{A-dA}$	view factor, Eq. (2)
$g$	acceleration of gravity
$H$	seat fire-to-ceiling distance
$h_L, h_U$	lower/upper surface heat transfer coefficient
$\tilde{h}$	dimensionless heat transfer coefficient, Eq. (12)
$k$	thermal conductivity
$N$	number of grid points in ceiling analysis
$\dot{Q}$	enthalpy flux in plume, Eq. (7)
$\dot{Q}^*$	dimensionless $\dot{Q}$ , Eq. (10)
$\dot{Q}_{equiv}$	equivalent fire strength
$\dot{Q}_{seat}$	strength of seat fire
$\dot{Q}'_i$	radiant heat transfer to wire per unit length
$\dot{Q}'_{amb-wire}$	radiation from ambient to wire
$\dot{Q}'_{ceiling-wire}$	radiation from ceiling to wire
$\dot{Q}'_{door-wire}$	radiation from doorway to wire
$\dot{Q}'_{wire}$	radiation from wire
$\dot{q}''_i$	rates of heat transfer per unit area
$\dot{q}''_{conv,U}, \dot{q}''_{conv,L}$	convection to upper/lower ceiling
$\dot{q}''_{door-ceiling}$	radiation from doorway to ceiling
$\dot{q}''_{rad-door}$	radiation from doorway
$\dot{q}''_{rad-seat}$	radiation from seat fire to ceiling
$\dot{q}''_{rerad,U}, \dot{q}''_{rerad,L}$	radiation from upper/lower ceiling

$\dot{q}_U''$ , $\dot{q}_L''$	net heat transfer to upper/lower ceiling
Re	Reynold's number, Eq. (12)
r	distance from plume impingement point
$T_{ad}$	adiabatic ceiling temperature, Eq. (9)
$T_{amb}$	ambient temperature
$T_{ign}$	ignition temperature
$T_{s,U}$ , $T_{s,L}$	upper/lower surface ceiling temperature
$T_w$	thermocouple wire temperature
t	time
$\alpha$	thermal diffusivity/wire configuration constant, Eq. (22)
$\beta$	a constant
$\Gamma_1$ , $\Gamma_2$	constants, Eq. (3)
$\delta Z$	indepth spacing of ceiling grid points
$\epsilon_U$ , $\epsilon_L$	lower/upper ceiling emissivity
$\theta$	configuration angle, Fig. 9
$\lambda_{r,seat}$	fraction of $\dot{Q}_{seat}$ radiated
$\nu$	kinematic viscosity
$\rho$	density
$\rho_{amb}$	density of ambient
$\sigma$	Stefan-Boltzmann constant

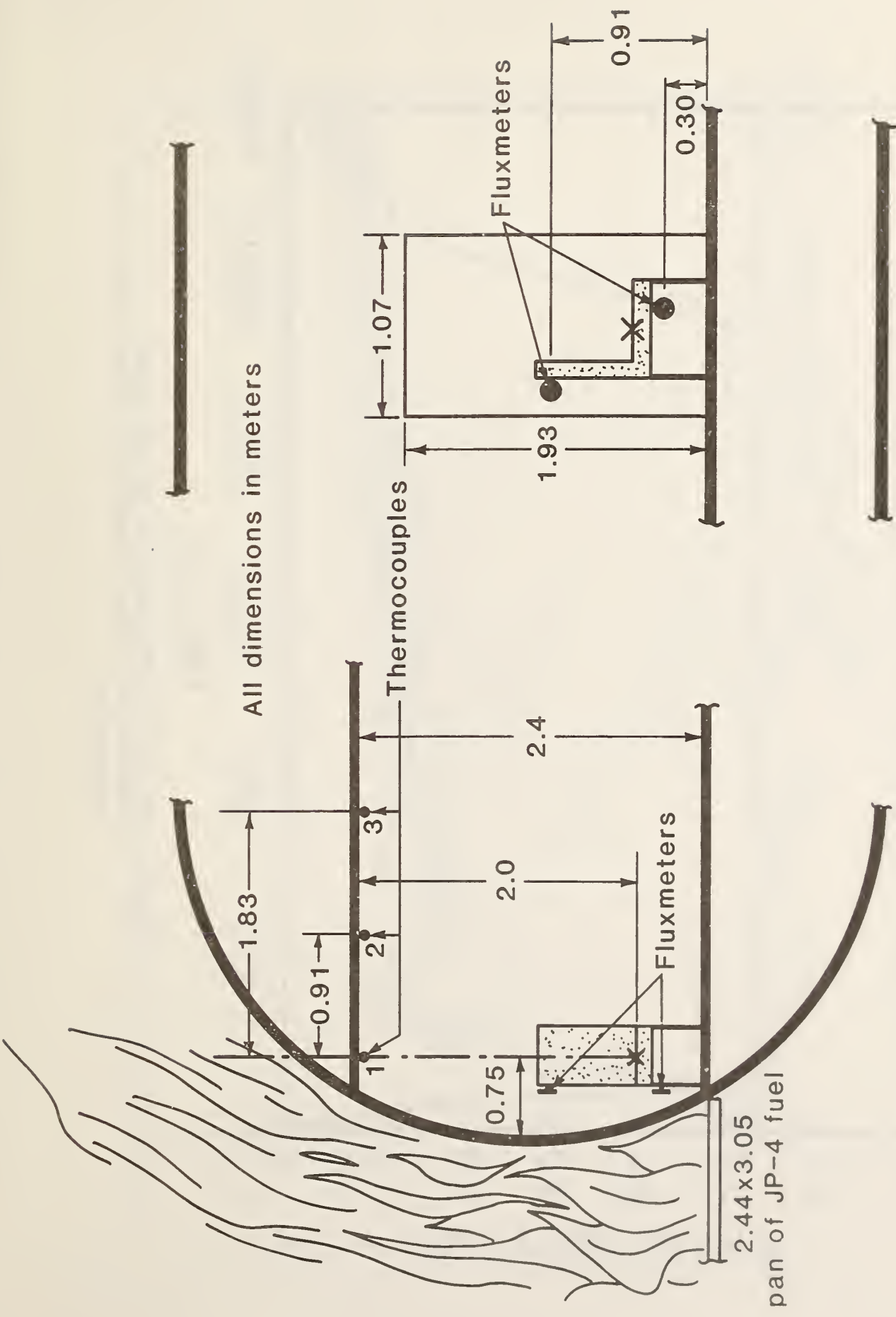


Figure 1. A schematic of the test setup

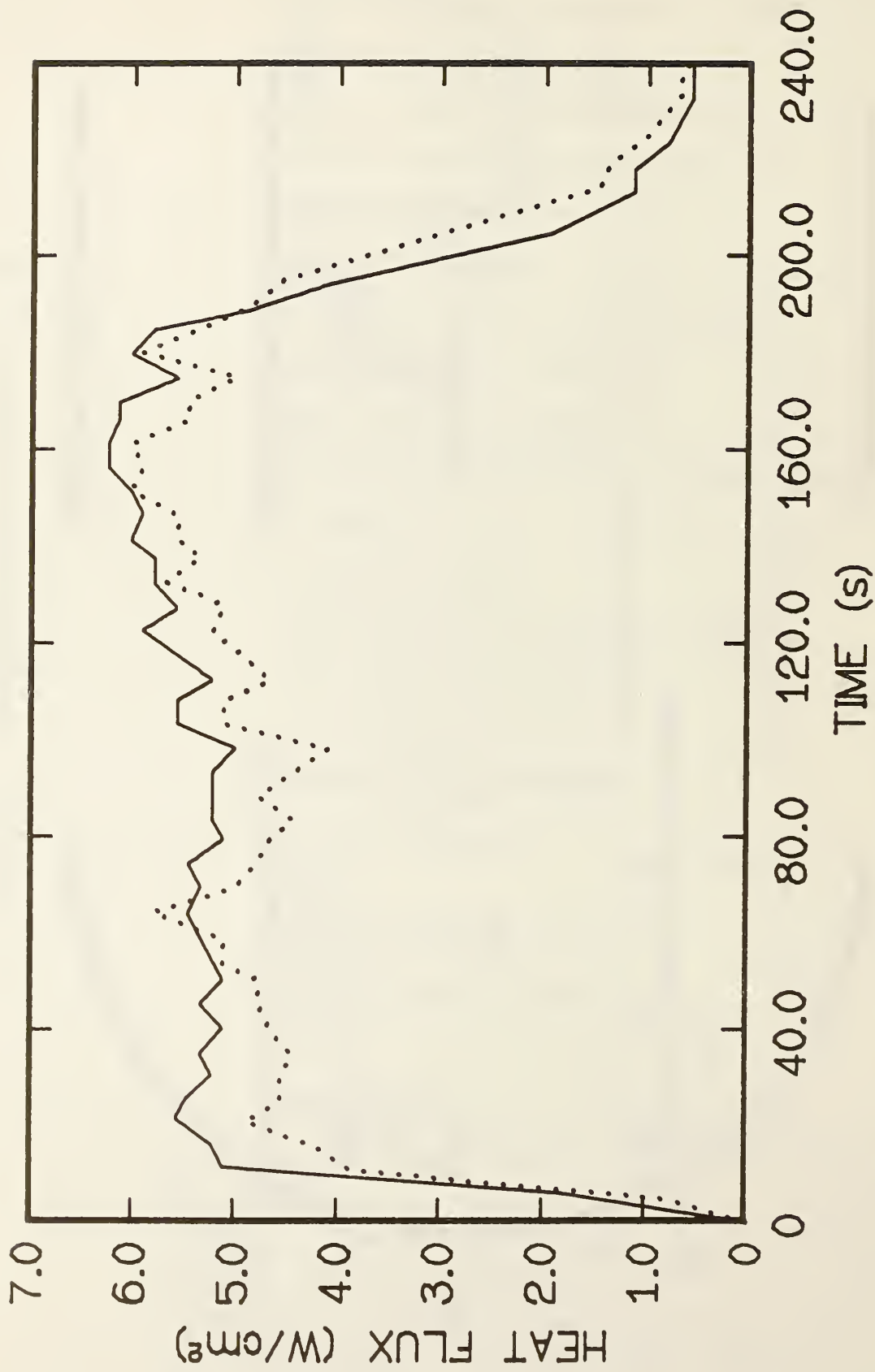


Figure 2. Measured doorway heat flux vs time (lower fluxmeter .....; upper fluxmeter \_\_\_\_\_); Test 111 (background)

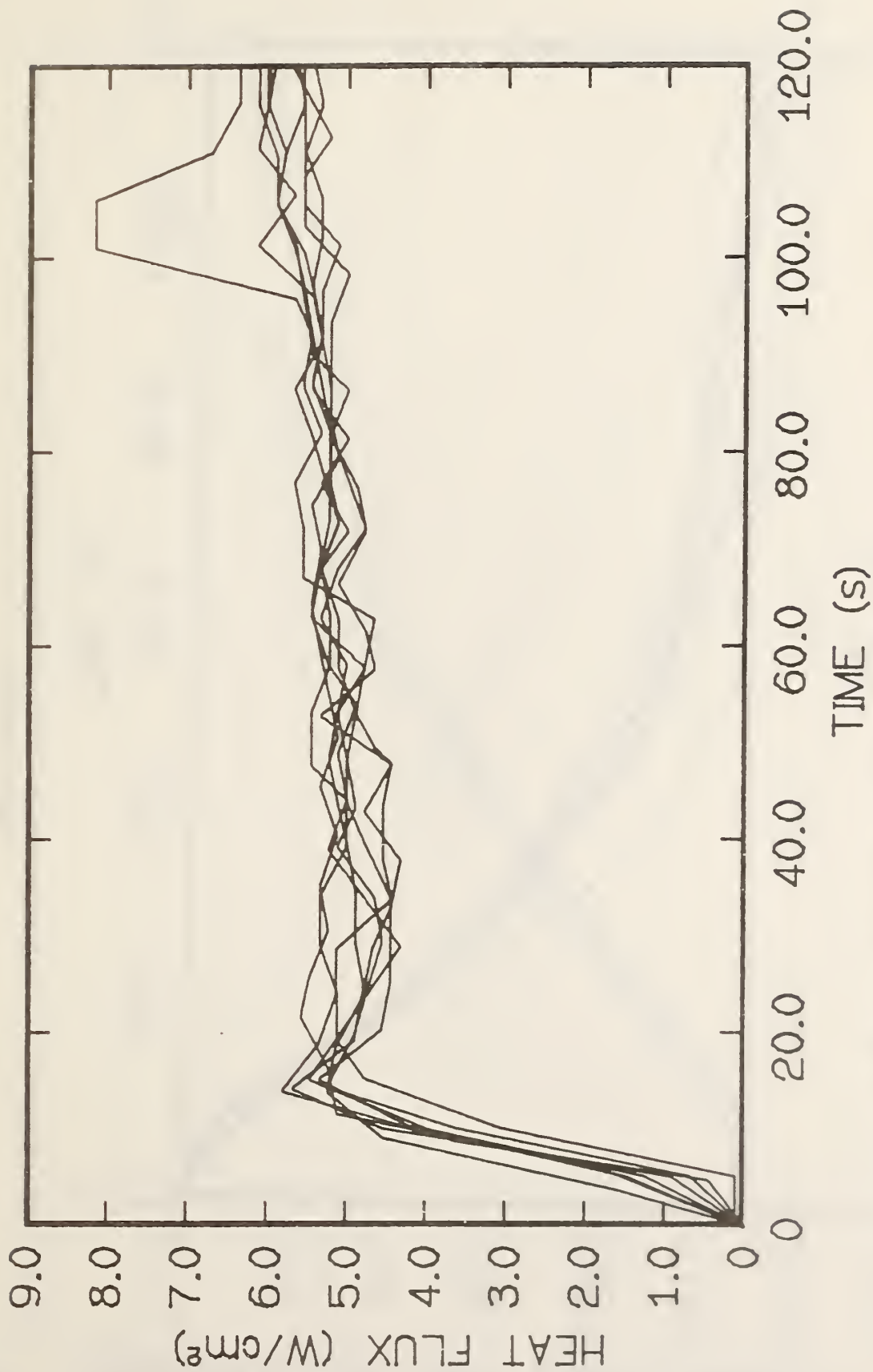


Figure 3. Measured doorway heat flux vs time (lower fluxmeter);  
Tests 104-111

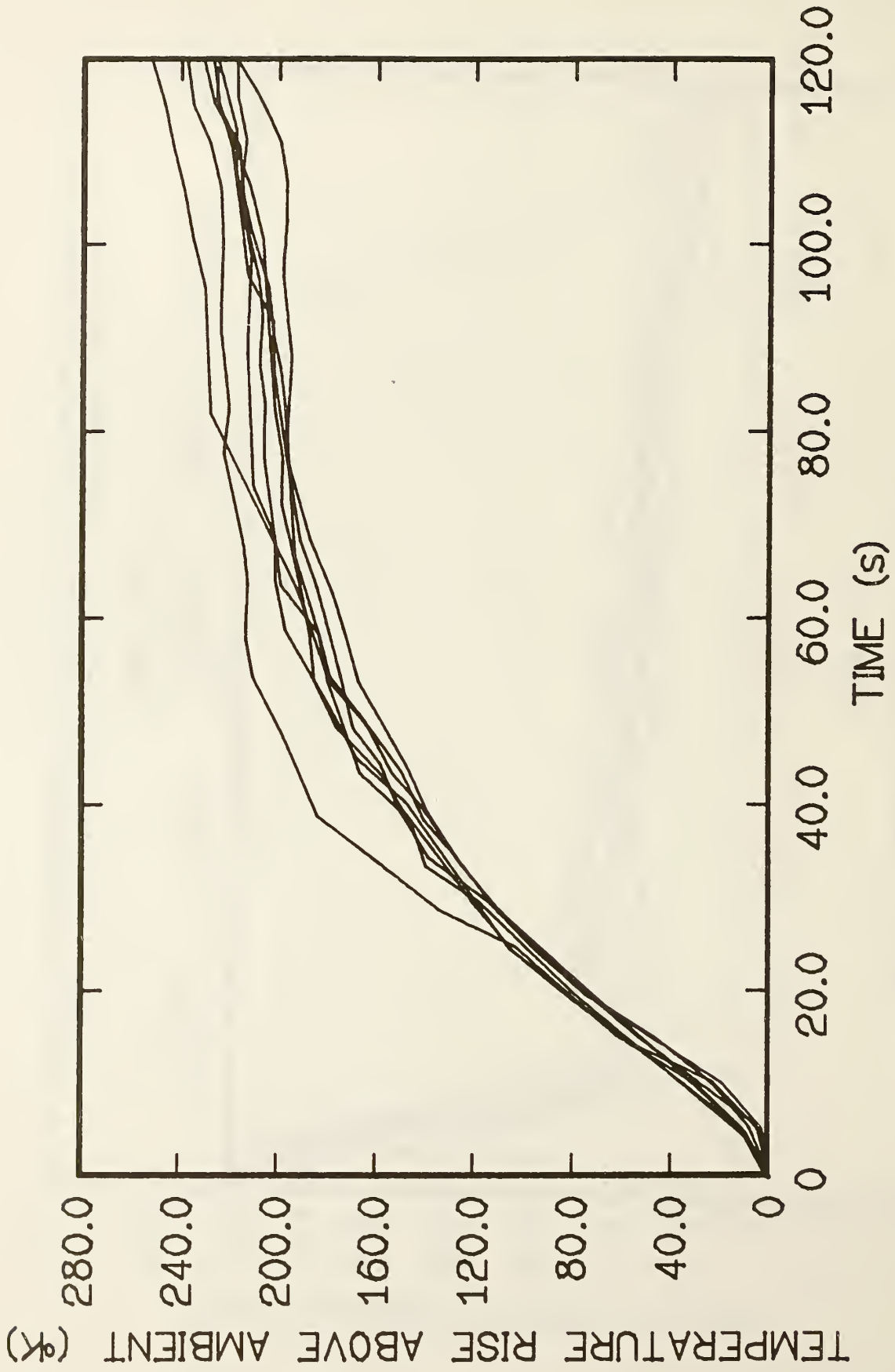


Figure 4. Measured temperature vs time at position 1;  
Tests 104-111

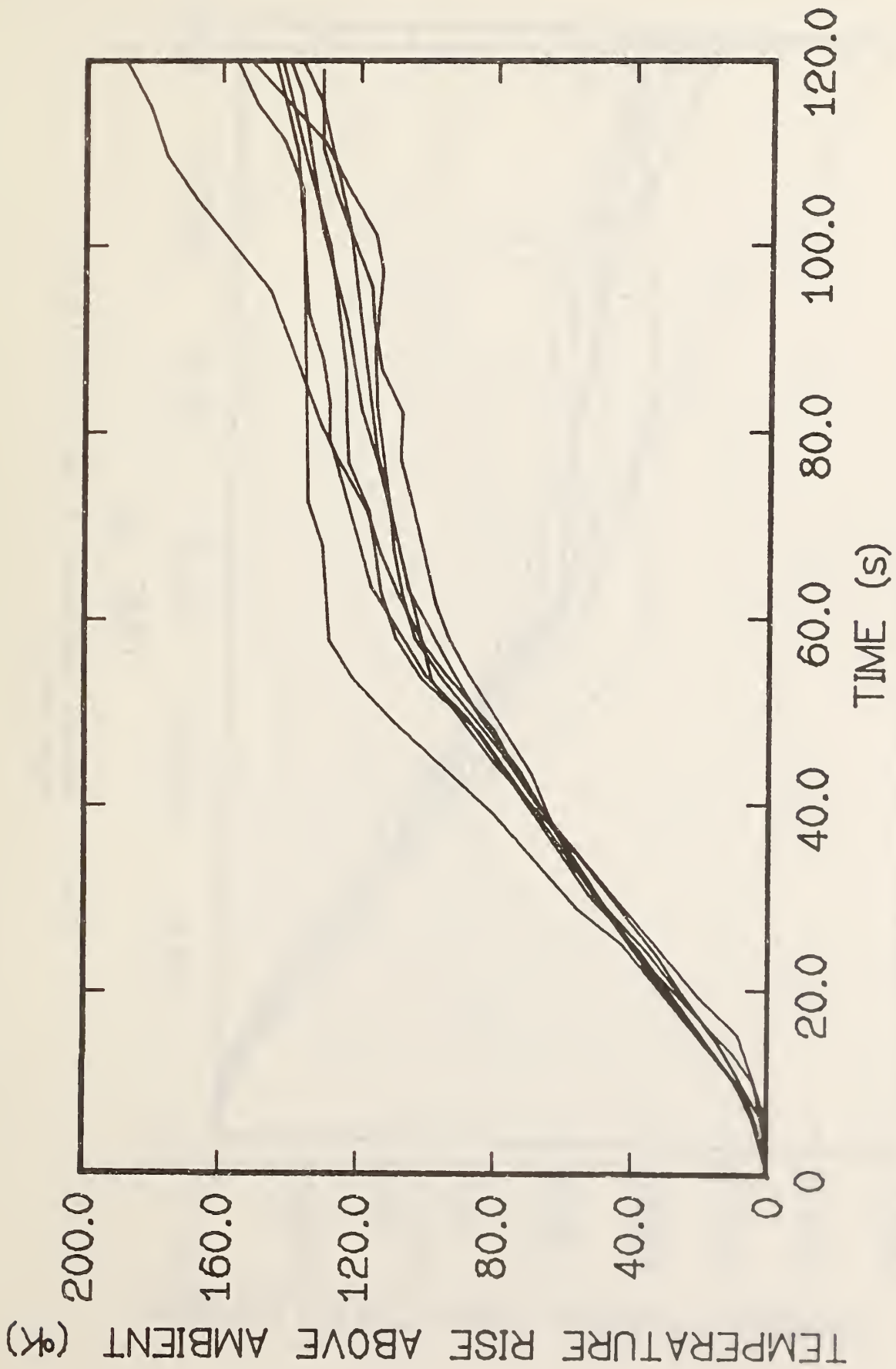


Figure 5. Measured temperature vs time at position 2;  
Tests 104-111

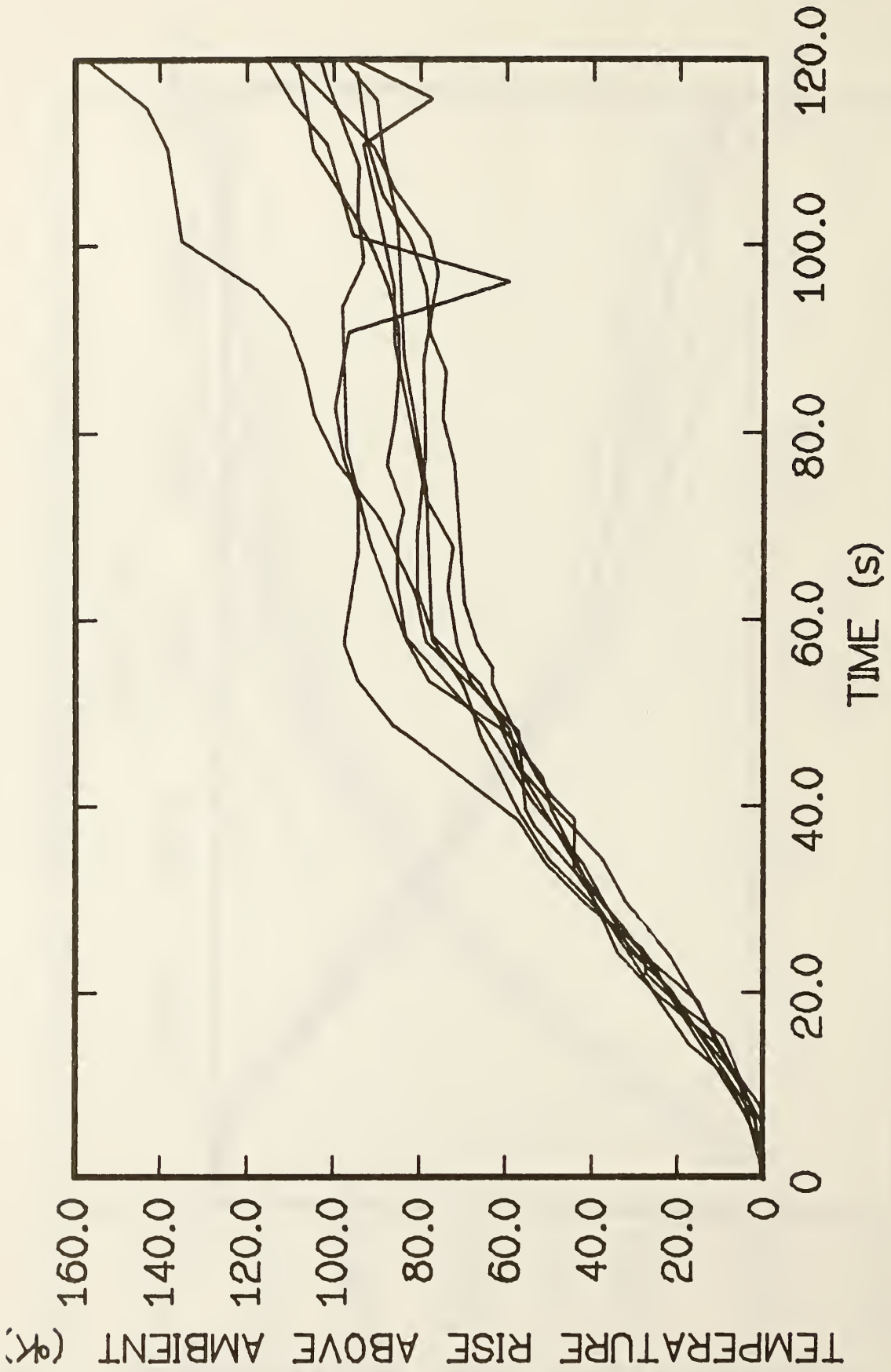


Figure 6. Measured temperature vs time at position 3;  
Tests 104-111

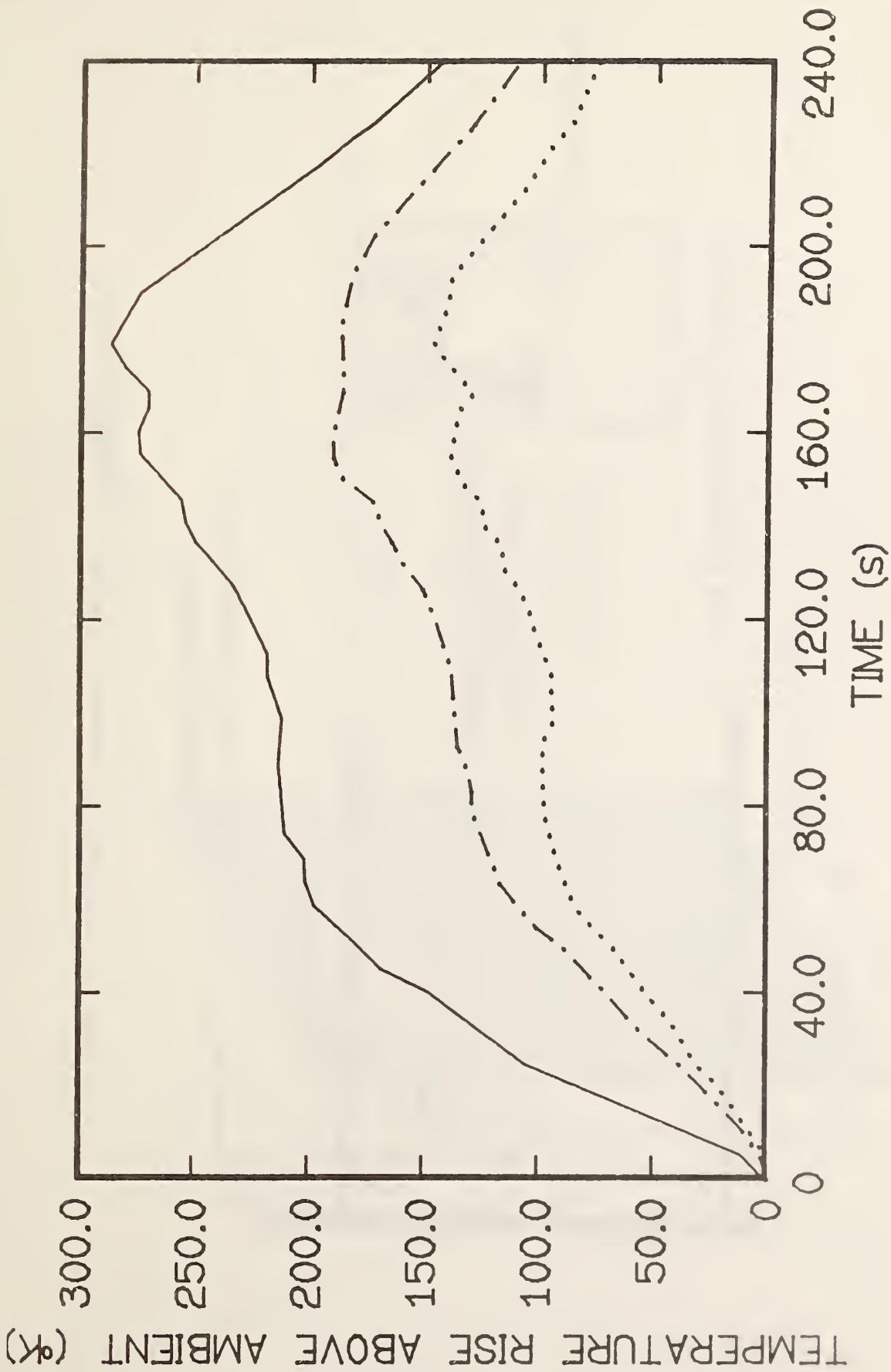


Figure 7. Measured temperature vs time at positions 1 (\_\_\_\_), 2 (\_\_\_\_), and 3 (.....); Test 111

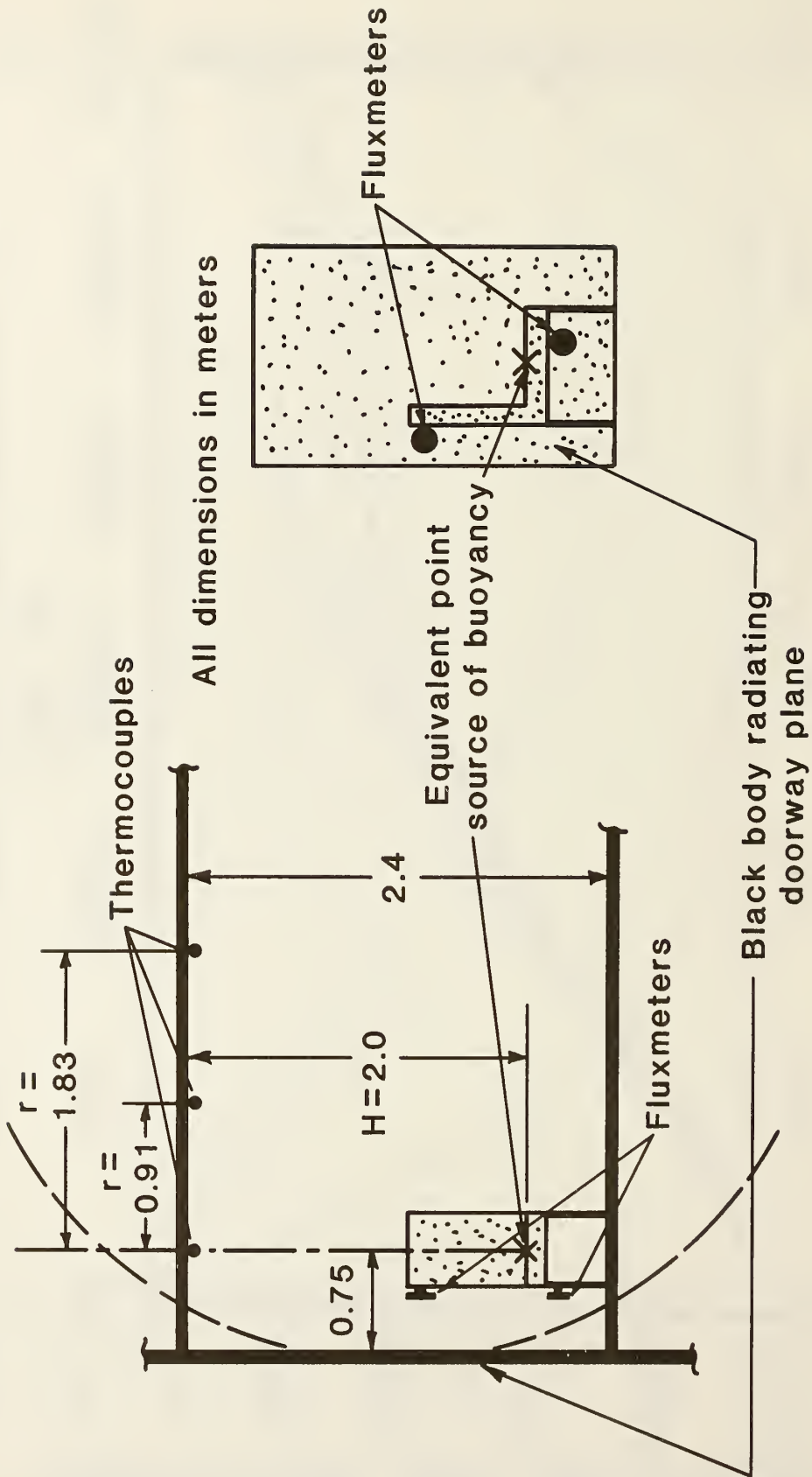


Figure 8. A simplified version of the post-crash fire scenario

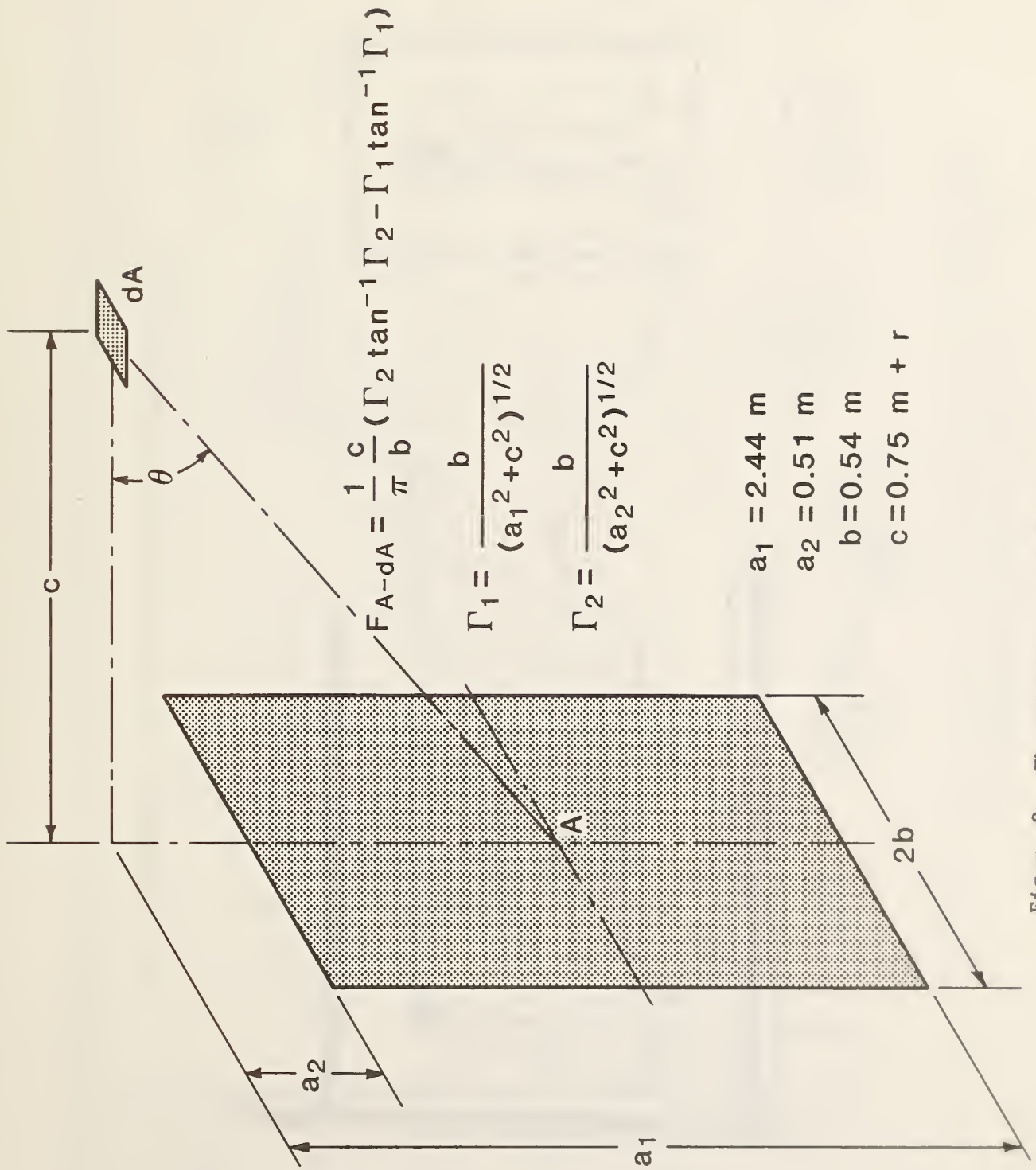


Figure 9. The viewfactor between the doorway and a ceiling element

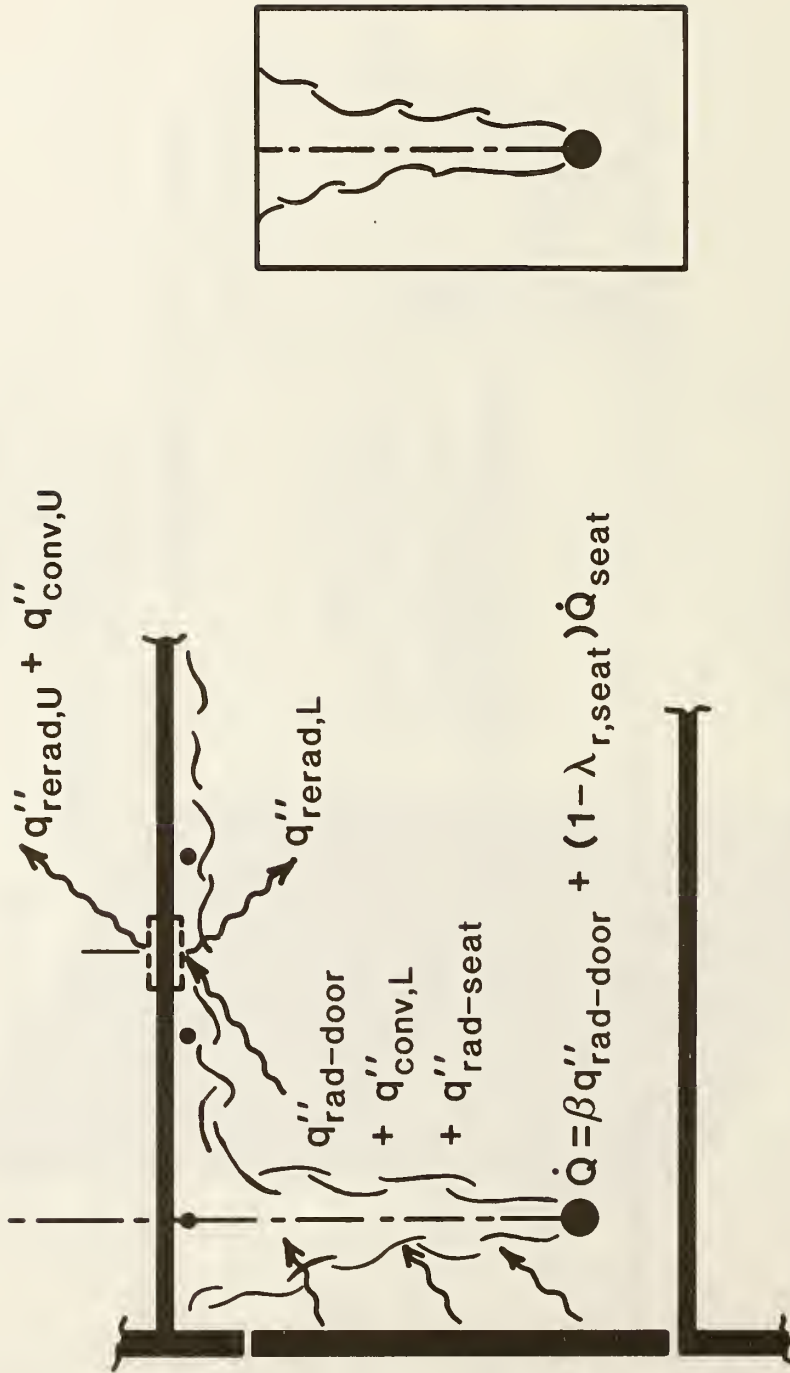


Figure 10. The idealized post-crash fire scenario

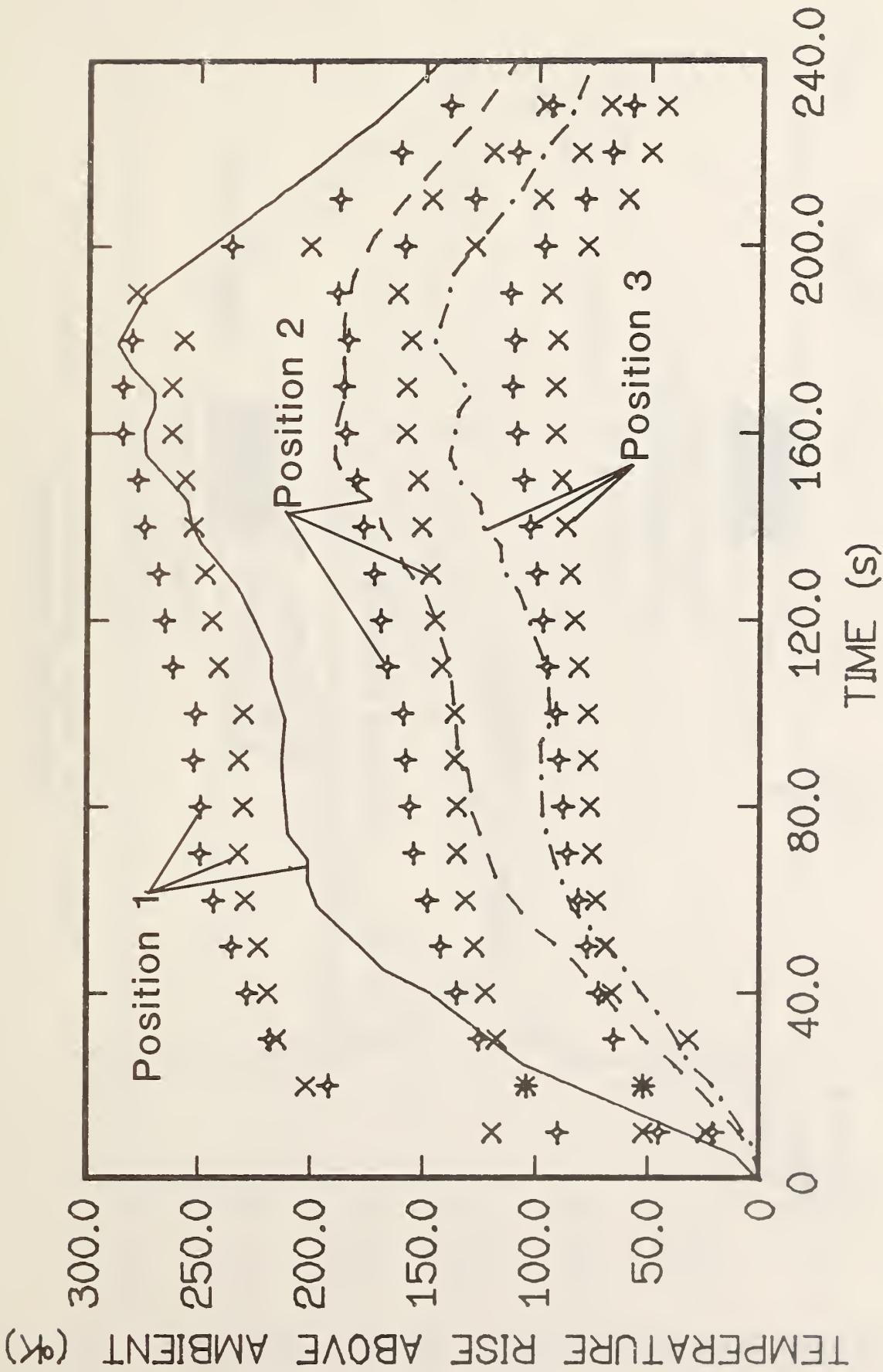


Figure 11. Computed Test 111 lower ceiling surface temperatures (+:  $\beta = 0$ ; x:  $\beta = 3.0 \text{ m}^2$ ) and corresponding, measured near-ceiling temperatures at positions 1, 2, and 3

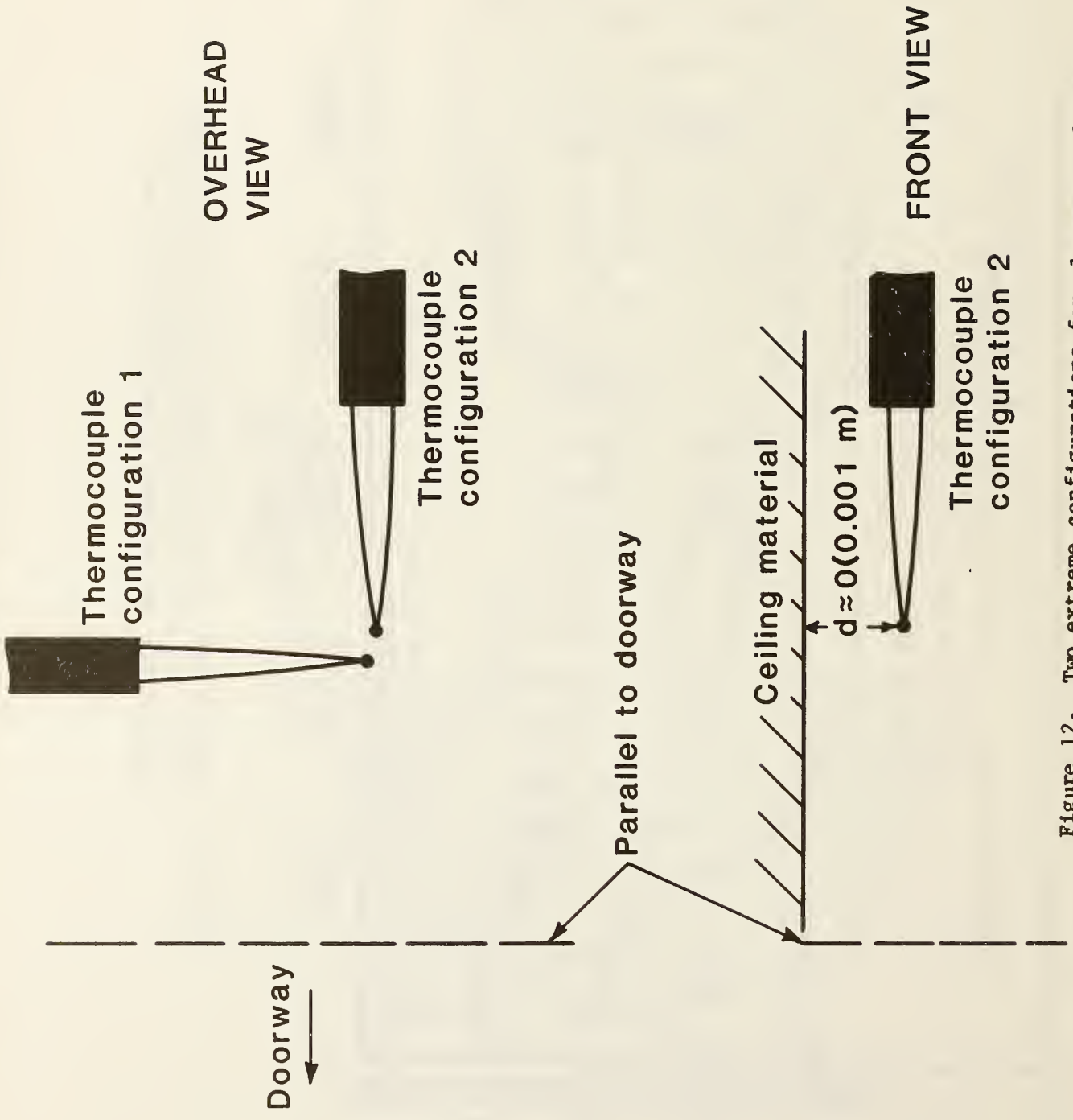


Figure 12. Two extreme configurations for placement of the near-ceiling thermocouples

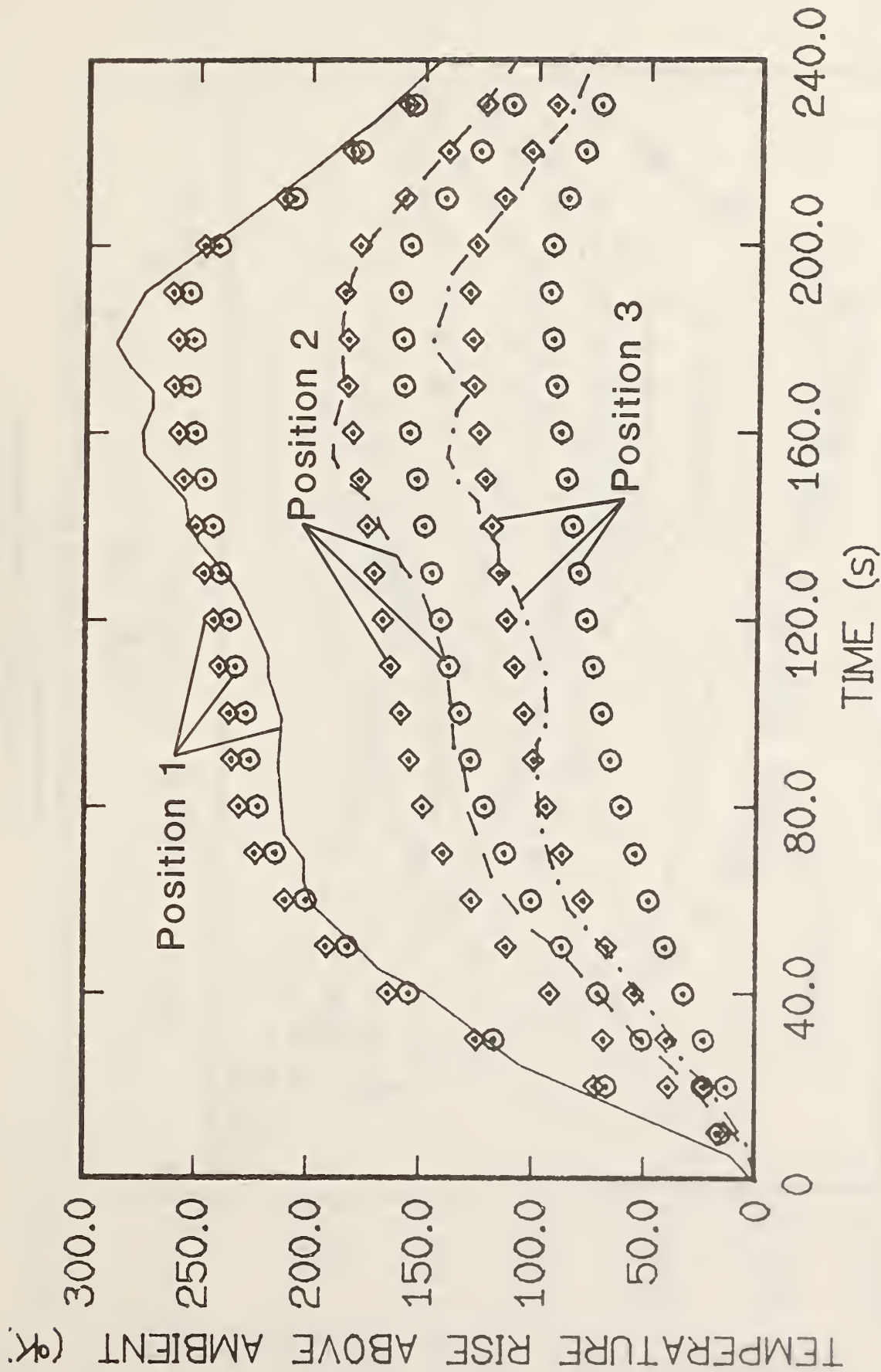


Figure 13. Predicted and measured Test 111 thermocouple temperatures ( $\beta = 2.0 \text{ m}^2$ ).  
 <>: predicted  $T_w$ , configuration 1  
 O: predicted  $T_w$ , configuration 2  
 —, — — —, — — — — —: measured  $T_w$



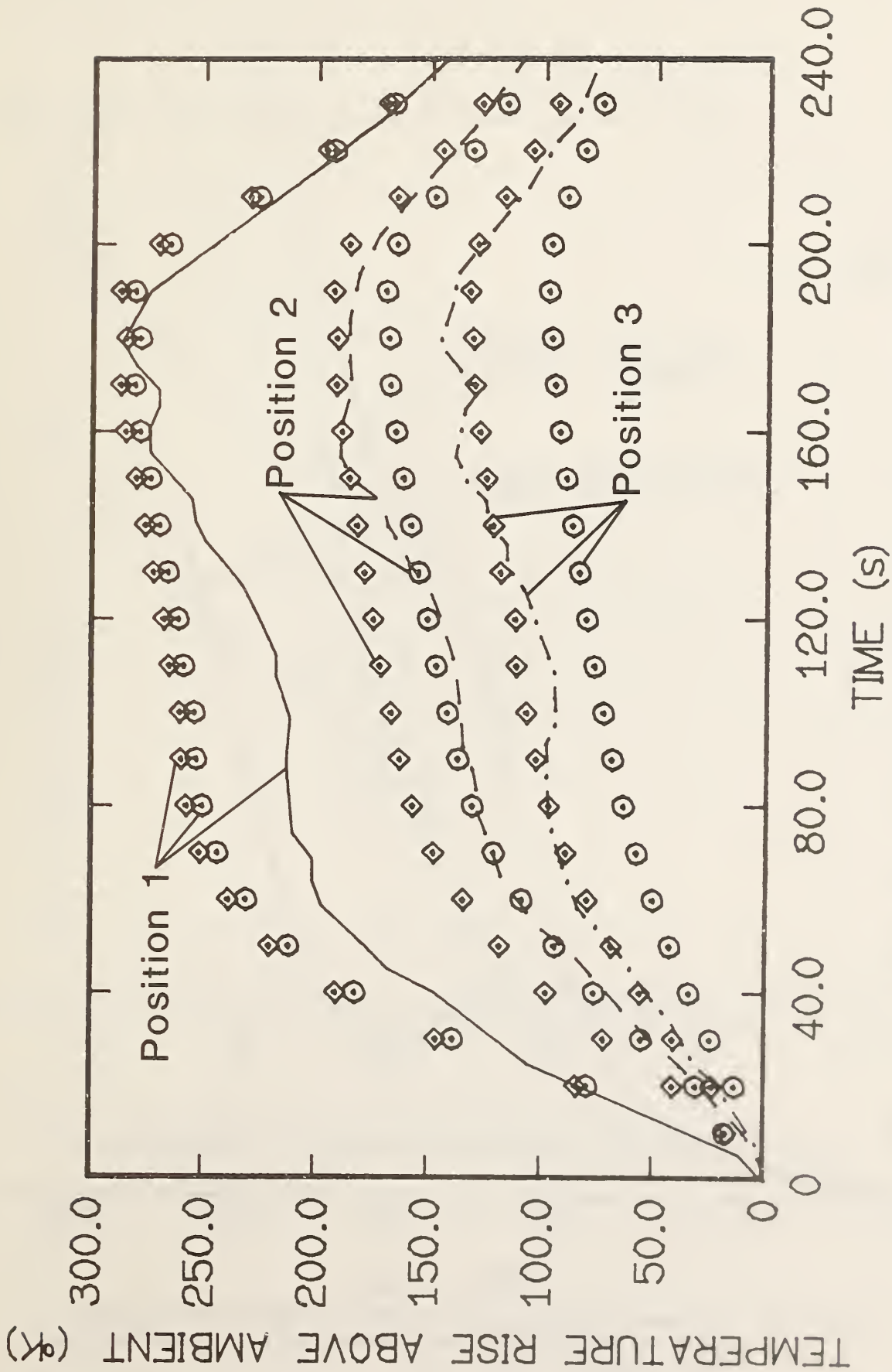


Figure 15. Predicted and measured Test 111 thermocouple temperatures ( $\beta = 4.0 \text{ m}^2$ ).

<>: predicted  $T_w$ , configuration 1  
 O: predicted  $T_w$ , configuration 2  
 —: measured  $T_w$

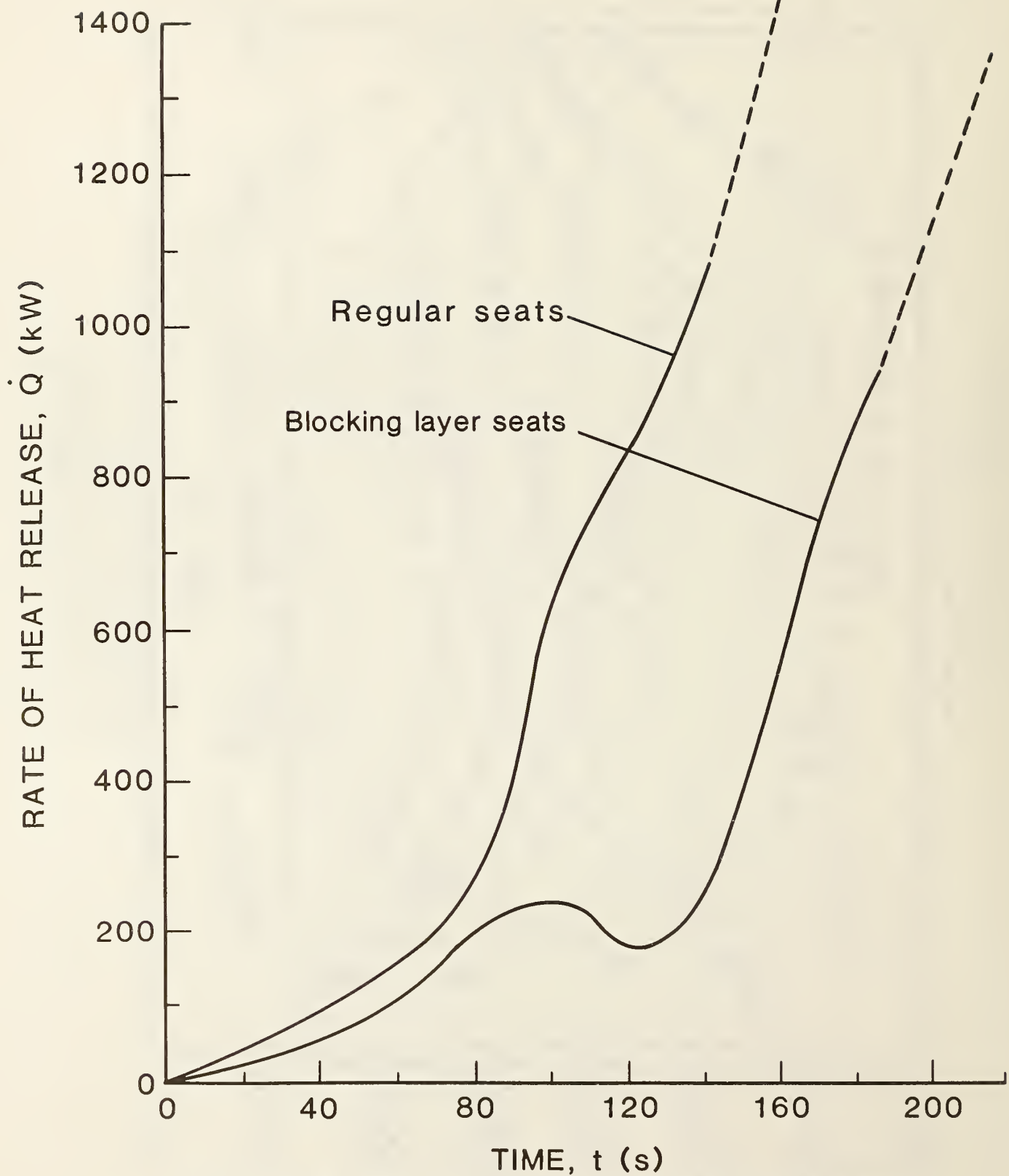


Figure 16. Estimate for  $\dot{Q}_{seat}$  for arrays of polyurethane seats with and without blocking layers [13] (--- extrapolated from curves of [13])

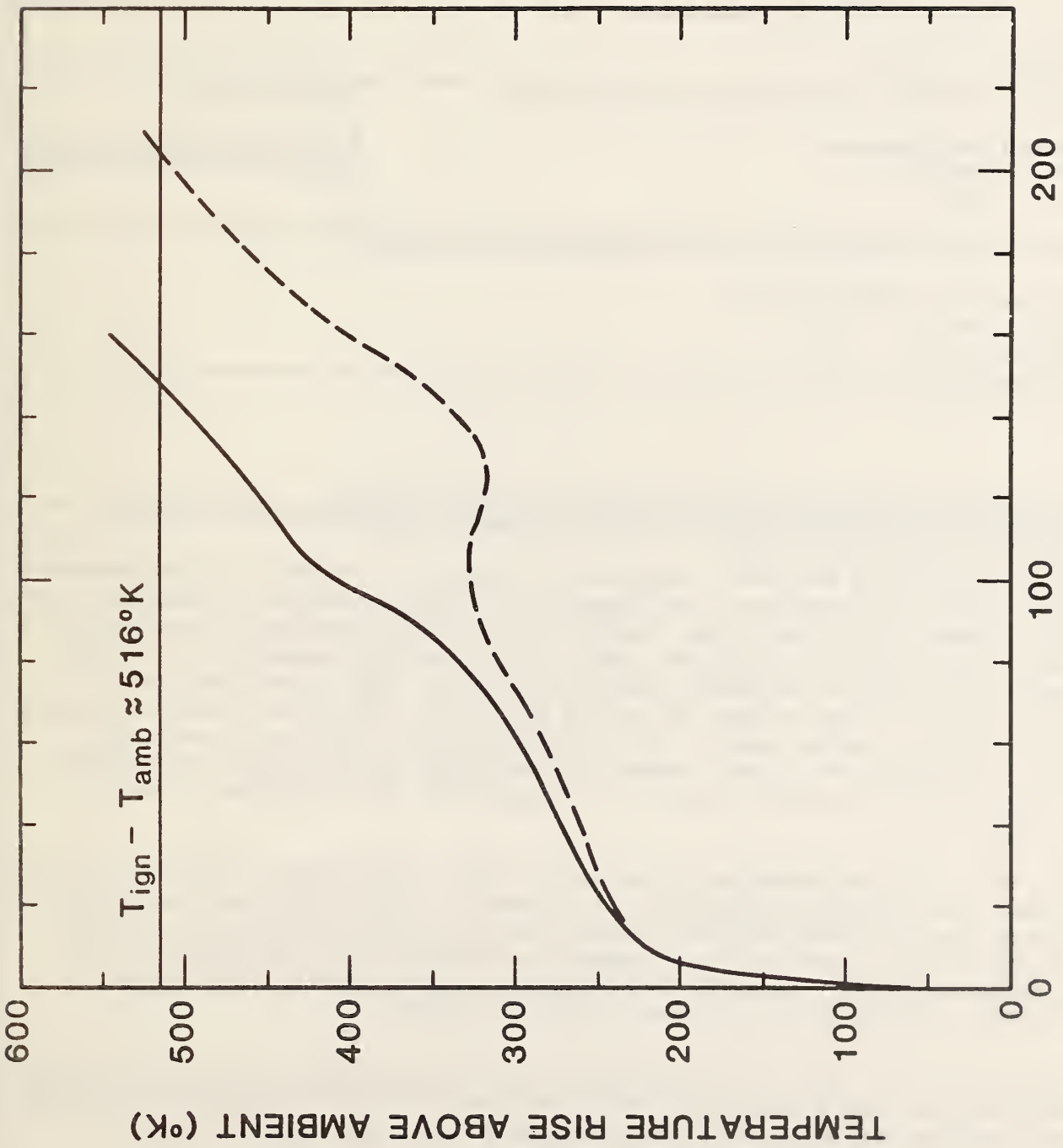


Figure 17. Predicted lower surface, post-crash, temperature of the honeycomb ceiling material in a cabin outfitted with polyurethane seat cushions; with (—) and without (---) blocking layers

U.S. DEPT. OF COMM. <b>BIBLIOGRAPHIC DATA SHEET</b> <i>(See Instructions)</i>	1. PUBLICATION OR REPORT NO.  NBSIR 84-2912	2. Performing Organ. Report No.	3. Publication Date  October 1984
4. TITLE AND SUBTITLE  The Thermal Response of Aircraft Cabin Ceiling Materials During a Post-Crash, External Fuel-Spill, Fire Scenario			
5. AUTHOR(S)  Leonard Y. Cooper			
6. PERFORMING ORGANIZATION <i>(If joint or other than NBS, see Instructions)</i>  NATIONAL BUREAU OF STANDARDS DEPARTMENT OF COMMERCE WASHINGTON, D.C. 20234			7. Contract/Grant No.  8. Type of Report & Period Covered
9. SPONSORING ORGANIZATION NAME AND COMPLETE ADDRESS <i>(Street, City, State, ZIP)</i>  Federal Aviation Administration Technical Center Atlantic City, N.J. 08405			
10. SUPPLEMENTARY NOTES  <input type="checkbox"/> Document describes a computer program; SF-185, FIPS Software Summary, is attached.			
11. ABSTRACT <i>(A 200-word or less factual summary of most significant information. If document includes a significant bibliography or literature survey, mention it here)</i>  An algorithm is developed to predict the thermal response of aircraft ceiling materials during a post-crash fire scenario. The scenario involves an aircraft's emergency exit doorway which opens directly onto the flames of an external, fuel-spill fire which engulf a large portion of the fuselage. Data of near-ceiling temperatures acquired during a series of eight, full-scale, wide-body aircraft cabin, post-crash test simulations provide indirect validation of the algorithm. These tests involved cabins outfitted with single, mockup seats. Two other full-scale cabin tests involving fire spread through twenty-one seat arrays with different types of seat construction provide the input data required to exercise the algorithm in evaluations of fully outfitted cabins.  Relative to the post-crash scenario, a measure of cabin fire safety is proposed, viz., the post-crash time-to-ceiling-ignition. This measure would be used as a surrogate for the post-crash time available for passengers to safely evacuate the cabin. In this sense, the algorithm is exercised in an example evaluation of the fire safety of a candidate honeycomb ceiling material used together in cabin systems involving polyurethane ceiling seating, with or without a blocking layer.			
12. KEY WORDS <i>(Six to twelve entries; alphabetical order; capitalize only proper names; and separate key words by semicolons)</i>  aircraft compartments; aircraft fires; algorithms; ceilings; egress; exits; fire safety; fire spread; upholstered furniture			
13. AVAILABILITY  <input checked="" type="checkbox"/> Unlimited <input type="checkbox"/> For Official Distribution. Do Not Release to NTIS <input type="checkbox"/> Order From Superintendent of Documents, U.S. Government Printing Office, Washington, D.C. 20402.  <input type="checkbox"/> Order From National Technical Information Service (NTIS), Springfield, VA. 22161			14. NO. OF PRINTED PAGES  52  15. Price  \$10.00



